Biomimetic Electrical Stimulation for Cardiac Tissue Engineering

by

Nina Tandon

B.E. Electrical Engineering
Cooper Union 2001

Submitted to the Department of Electrical Engineering and Computer Science in partial fulfillment of the requirements for the degree of

Master of Science in Electrical Engineering

at the
MASSACHUSETTS INSTITUTE OF TECHNOLOGY

August 2006

Author.....
Nina Tandon
Department of Electrical Engineering and Computer Science
August 11, 2006

Certified by.....
Joel Voldman, Co-Supervisor
Associate Professor of Electrical Engineering and Computer Science
Massachusetts Institute of Technology

Certified by.....
Gordana Vunjak-Novakovic, Co-Supervisor
Professor of Biomedical Engineering
Columbia University

Accepted by .....
Arthur C. Smith
Chairman, Department Committee for Graduate Students

Biomimetic Electrical Stimulation for Cardiac Tissue Engineering

by

Nina Tandon

Submitted to the Department of Electrical Engineering
and Computer Science on August 11, 2006 in partial fulfillment
of the requirements for the degree of
Master of Science in Electrical Engineering

ABSTRACT

A major challenge of tissue engineering is directing cells to establish the physiological structure and function of the tissue being replaced. Electrical stimulation has been used to induce synchronous contractions of cultured cardiac constructs. The hypothesis adopted for this study is that functional cardiac constructs can be engineered by "mimicking" the conditions present during cardiac development, and in particular, electrical stimulation using supra-threshold signals.

For this Master's Thesis research, I have compared the material properties and charge-transfer characteristics at the electrode-electrolyte interface of various biocompatible materials, including carbon, stainless steel, titanium and titanium nitride, for use as electrodes in a biomimetic system for cardiac tissue engineering. I have also designed and implemented an electrical stimulator which is capable of modulating several important parameters of electrical stimulation, including stimulus amplitude and frequency. In addition, I have built an experimental setup incorporating this electrical stimulator and used it for experiments with C2C12 mouse myoblast cells and neonatal rat cardiomyocytes. Lastly, I have analyzed cell morphology as well as functional performance of engineered tissue by assessing excitation thresholds and maximum capture rates.

Thesis Supervisors:

Joel Voldman
Associate Professor of Electrical Engineering and Computer Science
Massachusetts Institute of Technology

Gordana Vunjak-Novakovic
Professor of Biomedical Engineering
Columbia University

ACKNOWLEDGEMENTS

The work presented here, although written by me, is the compilation of the efforts of many people who guided and supported me along the way.

The idea of writing a "thesis" has been something I have been dreading, but my advisors Joel and Gordana have been so supportive—I feel so lucky to have been adopted by them. Gordana, that day in Starbucks, talking with you, I knew I was ready to take that deep breath and dive in--not a moment sooner. And Joel, you really made me feel like I had a home here in EECS for the first time.

Thank you Hyoungshin Park for really helping me to get started in the lab. Thank you for being patient with me, my ignorance, klutziness and many, many questions. Thank you Chris Cannizzarro for always being there to brainstorm with, and tinker with, and get late-night Indian food with, I owe you hugs beyond your hug limit. Thank you Elisa Figallo for staying up with me all those many nights taking measurements, trying to see deeper meaning in all those images. Thank you Sharon, Darja and Alex for all the laughs and advice.

I especially want to thank my parents, my sisters and my brother who have been a veritable springboard upon which to bounce ideas, or to just eat dinner, go shopping, or walk the dog. Thank you to my friends who have endured the long-silences and excuses of a grad student in the thesis-zone. In particular, thank you Shelagh, Carla, Carol, Ohad, Jay and Jessica.

Last but not least, thank you Franz and Stormie for helping me realize there is a world where there's always a reason to giggle. A lot.

TABLE OF CONTENTS

LIST OF FIGURES

INTRODUCTION

Over 7 million people in the United States have suffered from myocardial infarction, and our country's aging population will undoubtedly increase this number [1]. Myocardial infarction typically results in fibrotic scar formation and permanently impaired cardiac function because, after a massive cell loss due to ischemia, the myocardial tissue lacks intrinsic regenerative capability. Heart transplantation is the ultimate solution to end-stage heart failure, but is problematic due to the lack of organ donors and complications associated with immune suppressive treatments. New solutions are needed, therefore, to regenerate hearts damaged by cardiovascular disease, alleviate the shortage of heart donors, test new drugs, and study general cardiac tissue development and function. In the past few years, cardiac tissue engineering has emerged as a new and ambitious approach combining engineering techniques with cell biology and medicine. It has been suggested that to create a functional (synchronously contracting) cardiac patch, one may need to cultivate three-dimensional cell constructs in bioreactors designed to reproduce some of the conditions experienced by the cells in normal heart tissue [2].

A biomimetic approach to cardiac tissue engineering may be designed to recapitulate any number of aspects of the actual *in vivo* environment. An important property of vascularized tissues, for example, such as myocardium, is that cells receive oxygen via convection of blood through a capillary network and diffusion into the tissue space surrounding each capillary. Moreover, the oxygen-carrying capacity of blood is greatly enhanced by the presence of hemoglobin, a natural oxygen carrier. A biomimetic approach to cardiac tissue engineering may imitate these characteristics by crafting a convective-diffusive oxygen supply and providing oxygen carriers in the culture medium. In a recent study employing perfusion of culture medium through channeled scaffolds (to mimic the role of capillary network), and supplementation of oxygen carriers (to mimic the role of hemoglobin), for example, higher amounts of DNA and cardiac markers, including troponin I, and connexin-43 was observed, and constructs exhibited significantly better contractile properties as compared to control constructs [3].

In vivo, cells in the heart are also exposed to a cyclic stretch associated with the pumping action of the heart. In a recent study, a biomimetic system applying cyclical stretch to tissue engineered constructs rings of cardiac tissue was employed and these patches contracted more vigorously than unstretched patches [4]. Moreover, in native myocardium, these macroscopic synchronous contractions are induced by electrical signals from the heart's electrical conduction system, (see **Section 1.1.3** for details), and in another recent study, a biomimetic system designed deliver electric signals mimicking those in native heart tissue was shown to induce contraction of cardiac constructs cultured *in vitro* in response to a pulsatile electrical field. In addition, the investigators reported that electrical stimulation resulted in the progressive development of conductive and contractile properties characteristic of heart muscle after just 8 days of culture [5]. One important area of work implicated by this study was that of further optimizing the conditions of electrical stimulation.

For this study, therefore, I have focused on the electrical stimulation component of a biomimetic system designed to promote orderly coupling between electrical signals and cell contractions in a way similar to that in native myocardium [6]. More specifically, I have examined the material properties and charge-transfer characteristics at the electrode-electrolyte interface of various biocompatible materials, including carbon, stainless steel, titanium and titanium nitride. I have also designed and implemented an electrical stimulator which is capable of modulating several important parameters of electrical stimulation, including stimulus amplitude and frequency. In addition, I have built an experimental setup incorporating this electrical stimulator and used it for experiments with C2C12 mouse myoblast cells and neonatal rat cardiomyocytes. Lastly, I have analyzed functional performance of engineered tissue by assessing excitation thresholds and maximum capture rates, as well as cell morphology.

In this thesis document, I first provide a background covering native cardiac tissue (**Section 1.1**), as well as cardiac tissue engineering (**Section 1.2**) before covering basic principles of electric stimulation of cells (**Section 1.3**) and electrochemical behavior of stimulation materials (**Section 1.4**). Next, I give an overview of the experimental materials and methods employed in performing the studies described in this study, including those for cell preparation (**Section 2.1**), bioreactor assembly (**Section 2.2**), electrical characterization of the bioreactor

(**Section 2.3**), electrical stimulation of constructs (**Section 2.4**), and assessments (**Section 2.5)**. Next, I present and discuss the results obtained in this study for electrode characterization (**Section 3.1**) bioreactor and stimulator design (**Section 3.2**) and biological results (**Section 3.3**). Finally, I conclude with a summary and discussion of possible future work implicated by this study (**Section 4**).

This research is intended to contribute to the goal of engineering a cardiac muscle construct through elucidating the proven beneficial effect of electrical stimulation on cardiac myocytes cultured on scaffolds. This knowledge will hopefully inform future work involving optimization of the conditions of electrical stimulation for cardiac tissue engineering.

1. BACKGROUND

1.1. NATIVE CARDIAC TISSUE

A good cardiac patch should replace native myocardium and reproduce contractile function when implanted in situ. In order to do so, it should be composed of differentiated, aligned cardiac cells, exhibit tissue-like contractile function, and after implantation, survive and vascularize. A short review of cardiac tissue is therefore in order.

1.1.1. The Cardiac Myocyte

The myocardial cell population consists largely of cardiac myocytes that occupy approximately 90% of the myocardial mass [7]. By mass, 90% to 95% of the nonmyocyte fraction of cardiac cells consists of cardiac fibroblasts, which are mainly responsible for the synthesis of major extracellular matrix proteins in the heart, including fibrillar collagen types I and III and fibronectin [7]. Remaining cells are endothelial cells comprising the heart's vasculature. It is interesting to note, however, that in the normal adult mammalian myocardium, there is at least one capillary next to every cardiomyocyte, and so although the mass of cardiomyocytes in a mammalian heart is approximately 25 times that of cardiac endothelial cells, the smaller endothelial cells outnumber cardiomyocytes by 3:1 [8].

The cardiac myocyte may be considered the most physically active cell in the human body. It contracts constantly, perhaps 3 billion times or more in an average human lifespan. Moreover, it coordinates its beating activity with 3 billion other myocytes in the main pump of the human heart [9]. There are three main types of cardiomyocytes: The first, and perhaps the archetypal cell, is the ventricular cardiomyocyte, which is responsible for the powerful contractions that constantly pump blood throughout the body. Their counterparts in the atria, whose action facilitates filling of the ventricles, are similar, although atrial cells are long and slender, and also, by producing the hormone atrial natriuretic peptide, function as secretory cells. A third somewhat heterogeneous group of myocytes makes up the heart's impulse generation and conduction system—these cells are responsible for generation of the impulse and its precisely timed

distribution to the working cells of the chambers at the appropriate point in the cardiac cycle [9].

One of the most important features of myocardium is its high density of gap junctions, which are clusters of channels spanning the membranes of closely opposed cells [9]. Gap junctions also form the cell-to-cell pathways for direct transmission of chemical signals, which are of prime importance during development and differentiation [9]. Experiments have shown that the ultrastructure and protein composition of gap junctions isolated from rat ventricles are tissue specific, i.e., markedly different from gap junctions in the liver and lens [10]. Moreover, gap-junction variability within the heart itself also appears to contribute to the distinctive electrophysiological properties of different myocyte subsets in different regions of the heart [9]. Connexin43 is by far the most abundant gap-junction protein in the ventricles and atria of mammalian cardiomyocytes, although connexin40 and connexin45 are now known also to be locally expressed in specialized zones [9].

1.1.2. Electric Fields and Currents and Cardiac Development

The effects of current and voltage in biological systems are intertwined because the voltages across cell membranes and epithelia have their roots in ionic pumps, and these current loops generate electric fields, the magnitude of which depends on the resistance of the tissues in its path [11]. The presence of endogenous electric fields and currents in the developing vertebrate embryo has been widely documented [12]. The main roles for electric currents in embryonic cardiac development are hypothesized to revolve around directing cell migration during the development of the cardiac primitive streak, the development of cardiac left-right asymmetry, and the development of a cardiac synctium [12-14].

During gastrulation, occurring early in the development of animal embryos, the morphology of the embryo is dramatically restructured by cell migration. During gastrulation and the formation of the nervous system, it has been hypothesized that three-dimensional gradients of voltage provide coordinates for embryonic morphogenesis by providing a coarse guide for galvanotactic cell migration [15].

One of the most important features of the developing vertebrate heart is that of left-right asymmetry. Errors in the proper patterning of this axis are believed to

lead to congenital anomalies of the heart, often with profound clinical consequences [16]. It has been suggested that one of the earliest patterning roles for ion flux is in the emergence of the left–right axis. As early as 1956, it was reported that a DC electric current imposed across the chick blastoderm was able to induce a high number of cardiac reversals [15].

In addition to left-right asymmetry and directed cell migration, electric currents have also been implicated in the development of the cardiac synctium via the development of synchronous contractions of uncoupled, contracting, cells [14]. The mechanisms of this coordination are via partial and full depolarization of nearby cells and lead to the formation of low-resistance coupling junctions at the contact interface [17].

1.1.3. The Cardiac Electrical Conduction System

To produce a heartbeat, the contractile capabilities of the billions of myocytes that make up the heart must be synchronized not only physically, so as to transmit contractile forces from one cell to the next, but also electrically, so as to coordinate the spread of the wave of electrical activation. As stated in Section 1.1.1, there are two types of muscle cells in the heart: contractile cells comprising the majority of the atrial and ventricular tissues of the heart, which lead to contraction and generation of force or pressure, and conducting cells, which are specialized muscle cells that do not contribute significantly to the generation of force, but instead function to rapidly spread action potentials over the entire myocardium [18]. Conducting cells comprise the tissues of the sinoatrial (SA) node, the atrial internodal tracts, the atrioventricular (AV) node, the bundle of His, and the Purkinje system. Another specialized feature of the conducting muscles of the heart is their capacity to spontaneously generate action potentials [18].

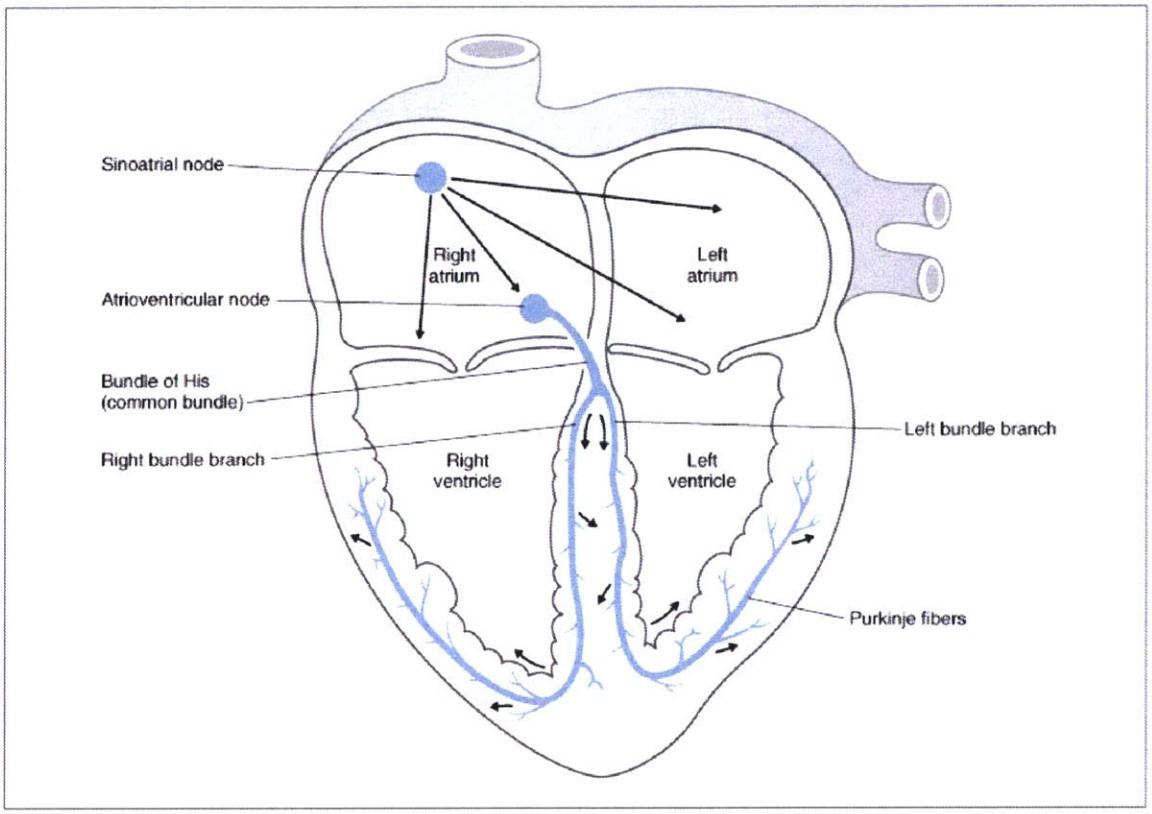

Figure 1: Schematic diagram showing the sequence of activation of the myocardium. The cardiac action potential is initiated in the sinoatrial node and spreads throughout the myocardium, as shown by the arrows. Figure is reprinted from [18].

Action potentials are electrical potentials (voltages) which have their origin in membrane potentials. Changes in membrane potential are caused by the flow of ions into or out of the cell, where differences in the concentrations of positive and negative ions give a localized separation of charges [18]. Normally, as shown in **Figure 1**, the action potential of the heart is initiated in the SA node, which serves as the pacemaker, and from there it spreads to the right and left atria via the atrial internodal tracts. Simultaneously, it is conducted to the AV node. From the AV node the action potential is distributed to the ventricles via the bundle of His, the main bundle branches to each ventricle, and Purkinje system [9, 18]. Rapid conduction of action potentials is facilitated by the presence of gap junctions.

An important feature of the cardiac electrical conduction system is that conduction properties in myocardium are anisotropic, with more rapid conduction in the direction parallel to the myocardial fiber axis than in the transverse direction. In fact, in normal ventricular myocardium, conduction in the direction

parallel to the long axis of the myocardial fiber bundles is approximately three times more rapid than in the transverse direction [19]. This property is attributable principally to the higher conductivity of myocardium in the longitudinal direction, in comparison to the transverse. Morphologically, this difference in conduction is due to the elongation of the myocardial cells—the action potential's pathway encounters fewer cell boundaries per unit distance in the longitudinal direction, in comparison to the transverse [19].

1.1.4. The Injured and Repairing Myocardium

One of the goals of a cardiac tissue engineered patch is to aid those who have suffered from myocardial infarction, and so a brief description of the mechanisms of injury and repair in the heart is in order. After non-fatal myocardial infarction, the inflammatory response is activated. Cytokine elaboration is particularly active after myocardial infarction and contributes to cardiac remodeling [20]. Acutely, cytokines contribute to survival or deaths of myocytes, modulation of cardiac contractility, alterations of vascular endothelium, and recruitment of additional circulating cells of inflammation to the injured myocardium, which leads to further local oxidative stress and remodeling but also initiates the processes of wound healing. Chronically, cytokines can mediate repair and remodeling through activating matrix metalloproteinases and collagen formation, and regulating integrins and angiogenesis and progenitor cell mobilization [20].

The loss of the normal ordered distribution of connexin43 gap junctions is particularly conspicuous in the myocardial zone bordering infarct scar tissue, where gap junctions are scattered extensively over myocyte surfaces, creating blocked tissue, and contributing to arrhythmia [21]. Clearly ordered intercalated disk arrays remain intact in zones distant from the infarct zone, however [21]. In addition, action potential prolongation, which is the result of functional downregulation of K currents, and aberrant Ca^{2+} handling is also a recurrent theme [22].

The deposition of a fibrotic connective tissue scar after infarction distorts the normal relationship of the surviving myocardial fiber bundles, since the connective tissue may invade and separate muscle fibers [23]. This separation results in a disruption of the normally well-defined directional differences in

impulse propagation, and may contribute to the occurrence of chronic arrhythmias in healed infarcts.

1.2. CARDIAC TISSUE ENGINEERING

The field of cardiac tissue engineering was motivated by the limited ability of the myocardium to regenerate after injury and the shortage of organs for transplantation. As a replacement for native myocardium, engineered heart tissue should therefore reproduce contractile function when implanted *in situ*. In order to accomplish this basic functionality, engineered myocardium should be composed of differentiated, aligned cardiac cells, exhibit tissue-like contractile function, and, after implantation, survive and vascularize.

The first efforts to regenerate functional myocardial tissue in the mid 1990s adopted the strategy of cell injection [2]. The proof-of-principle experiments of cardiac cell implantation in the heart were first achieved a decade ago using genetically selected embryonic stem cell-derived cardiomyocytes [2]. In 2001, Kocher et al. reported that the implantation of human bone-marrow derived angioblasts could improve cardiac function [24]. Although these studies reported being able to improve contractile function, high percentages of the injected cell suspension (over 90%) have been reported to be lost and did not engraft [2]. This finding suggests that functional integration of the injected cells might not be required in order to achieve a beneficial effect on cardiac function, and that the improvement results from some other mechanism such as inducement of neovascularization and subsequent increases in perfusion[24]. Nonetheless, because the injected cells showed poor alignment, increasing the risk for arrhythmia, and poor differentiation, they are not considered useful as engineered cardiac tissue.

The concept of tissue engineering using three-dimensional scaffolds has certain advantages over the direct injection of cells for the repair of the wounded heart. Firstly, the scaffolds themselves may replace the missing or damaged extracellular matrix in the infarcted area and provide temporary support for the cells repairing the wound, whether implanted or from the host. Furthermore, while producing a tissue-engineered construct, one may control the size, shape, elasticity and strength of the graft *in vitro*, and improve the engraftment ratio,

alignment, and differentiation of implanted cells, in addition to increasing the size of engineered tissue to a useful clinical size and improving the contractile function of an implanted cardiac graft.

A variety of studies have been undertaken using an assortment of synthetic biodegradable scaffolds with different types of cells, in which the engineered tissue for implantation would be cultured under conditions improving contractile function, differentiation and alignment. Several groups have reported encouraging results with various techniques for constructing beating cardiac patches for transplantation. Shimizu et al. grew rat cardiomyocytes on polymer surfaces that promoted the detachment of the thin cell layers when the temperature was reduced [25]. They implanted four such fused layers and implanted the "patch" subcutaneously in a rat. The patch survived, was vascularized, and was still beating six months later, but is still too small to be considered of clinical relevance [25]. Eschenhagen et al. created rings of cardiac tissue using cardiomyocytes from neonatal rats to which they applied cyclical stretch. Zimmerman et al. showed that these patches contracted more vigorously than unstretched patches [4]. Although the application of mechanical stretch improved cell differentiation and the force of contraction, the distribution of gap junctions remained disorganized, and cells were missing M-bands and intercalated discs, which are important features of differentiated cardiac tissue [5].

Costa et al., while investigating the generation of electrical and mechanical anisotropy in engineered heart tissue, showed that fibroblasts, previously thought to align randomly and independently of geometry, in fact align according to the free edges of gels [18]. This result suggests that the presence of voids and free surfaces such as the endocardium and epicardium, cleavage planes, and blood vessels, may play a role in governing cell and fiber alignment in developing and remodeling myocardium, myocardial scar tissue, and engineered heart constructs. Their study, however, did not investigate the alignment of cardiomyocytes themselves.

Recently, Radisic et al. reported improved functional assembly of engineered myocardium by culturing myocardium in the presence of suprathreshold pulsatile electric fields. They were able to induce a remarkable enhancement of cell

alignment and coupling, synchronous construct contractions, and ultrastructual organization [5]. They did not, however, investigate whether the alignment induced in their engineered cardiac patches produced any level of electrical anisotropy. Moreover, they did not report any optimization of the electric field stimulus.

This study will adopt a similar methodology to that undertaken by Radisic et al., and will focus on the investigation of the functional performance of engineered cardiac tissue constructs through the use of modulated electric fields for cardiac tissue engineering.

1.3. ELECTRICAL STIMULATION OF CELLS

Tissue in general, including excitable tissue, is surrounded by extracellular fluid with relatively high conductivity (3-12 mS/cm) [26]. In vitro, this case holds as well, since the conductivity of the culture medium is comparable to that of extracellular fluid (15 mS/cm). Since the electrodes used for stimulation are placed in this conductor composed of this fluid, it is essential to understand how the currents and electric fields are distributed within it, under normal and stimulated conditions.

1.3.1. Electroquasistatic Formulation

In simple cases such as a homogenous, isotropic medium, and where the system under consideration is much smaller than the wavelengths of interest (for biological systems generally under 10 kHz), the calculation of the electric fields can be performed by solving Maxwell's equations, assuming electroquasistatic conditions [26]. The electroquasitatatic formulation is as follows:

Conservation of Charge:	$\nabla \cdot \mathbf{J} = 0$	(Eq. 1.3.1.1)
Gauss' Law:	$\nabla \cdot \mathbf{E} = \frac{\rho}{\varepsilon}$	(Eq. 1.3.1.2)
Ohm's Law for conductors:	$\mathbf{J} = \sigma \mathbf{E}$	(Eq. 1.3.1.3)
Electric Field:	$\mathbf{E} = -\nabla \phi$	(Eq. 1.3.1.4)

Where $\mathbf{E}$ is the electric field (V/m) defined as the negative gradient of the scalar potential ϕ; $\mathbf{J}$ is the current density (A/m); σ is the conductivity (S/m); ρ is the

charge density (C/m^3); ε is the permittivity of the medium (F/m); and $\nabla \cdot \mathbf{A}$ is the divergence of the vector $\mathbf{A}$.

In any electrochemical system, a change in electrical potential occurs upon crossing from one conducting phase to another (from the metal electrode to the electrolyte) at the interface itself, in a very narrow interphase region, thus forming an electric field (measured in V/m) at the interface. This change in potential exists even in the equilibrium condition (no current) [27]. Electrochemical reactions may occur in this interphase region if the electrical potential profile is forced away from the equilibrium condition. In the absence of current, the electrical potential is constant (no gradient) throughout the electrolyte beyond the narrow interphase region. During current flow, a potential gradient exists in the electrolyte, generally many orders of magnitude smaller than at the interface [27]. Assuming electroquasistatic conditions, the electric field lines in this system will resemble those of a standard electric dipole [26].

1.3.2. Physiologic parameter ranges for endogenous electric-fields

Historically, there has been a much longer association of electricity with death than life. Zeus, for example, hurled thunderbolts to destroy his enemies, not revive them. The association between electricity and life, however, was discovered in 1786, when Luigi Galvani, a professor of anatomy and surgery at the University of Bologna, was researching a dissected frog in his laboratory as a thunderstorm raged outside. To his surprise, the frog's leg muscle twitched whenever his scissors touched a nerve, and he wondered if through the air, the lightning could have exerted some subtle influence on the frog's nerves and muscles [28]. It is now of course widely known that not only are many cells within the body sensitive to electrical stimuli, but that the body also generates much electricity during daily life.

For vertebrates, the physiologically significant range of endogenously produced electric field strengths is likely to be between 0.1-10 V/cm: 1-2 V/cm fields have been measured on either side of the cut surface of wounds, for example, owing to either ion flux through leaky cell membranes or transepithelial potential driven by Na+ pumps [29]. Similarly, fields of 0.4-1.4 V/cm have been measured during injuries to bovine cornea, and guinea pig and human skin, respectively [30].

In addition to injuries being a source of electricity, the beating heart is a large bioelectrical source in the body, but whether or not this presents a source of endogenous electrical stimulation is unknown, and so measured endogenous potentials due to heart-induced electrical stimulation may present a lower limit to physiologically relevant electrical stimulation levels. Peak-to-peak electric fields inside a rat's chest due to cardiac function were found by Miller and Creim to be between 0.02 and 0.03 V/cm, and Hart and Gandhi have calculated that this field can reach other organs in the body such as the lungs, stomach, and liver at the same order of magnitude or one below [31].

1.3.3. Mechanisms of applied electric-field stimulation

The electric charges in a physiologic medium are carried by ions and those in traditional electric circuitry and electrodes by electrons. At the interface is a transduction of charge carriers from electrons to ions. During an applied stimulus to a physiologic medium, a redistribution of charge occurs: at the interface that is driven negative, the metal electrode has an excess of negative charge. This will attract positive charge (cations) in solution towards the electrode and repel negative charge (anions). At the second electrode, the opposite processes occur, i.e. the repulsion of anions by the negative electrode is countered by attraction of anions at the positive electrode. In the interfacial region and bulk solution, there will be net electroneutrality [27]. The application of electrical stimulation thus induces hyperpolarization at the anode end of the cell and depolarization at the cathode end of the cell [32]

In addition to hyperpolarization, intense electric fields may stimulate cells via electroporation of the cell membrane, by causing the cellular membrane potential to increase to levels above 300 mV, as associated with defibrillation of the heart [33] and DNA transfection. Other possible mechanisms for electric field stimulation are via the alteration of receptor conformations, motion of receptors or channels with the cellular membrane via electrophoresis, or activation of calcium channels [29].

1.4. ELECTROCHEMICAL BEHAVIOR OF STIMULATION MATERIALS

When compounds are lacking in biocompatibility, the recipient of an implant may experience long-lasting chronic inflammation, exposure to cytotoxic chemicals, and the implanted device itself may be corroded. Progress in material and coating technologies have brought forth a number of materials suitable for electrostimulation and sensing applications, in addition to stainless steel. These include titanium nitrides, titanium as a substrate material, and different forms of carbon.

1.4.1. Porous Carbon

Carbon exhibits a unique ability to form a wide variety of structures [34] including Buckeyballs, nanotubes, graphite and diamond. The carbon rod electrodes utilized in this study are engineered for high-current density since their main application is in carbon rod evaporation systems for electron microscopy, and for carbon nanotube generation. Such carbon is extremely pure (< 2ppm other elements) [35, 36].

The electrochemical behavior of carbon electrodes is closely tied to the amount of surface area the electrode presents to the electrolyte. Nanoporous carbon electrodes, for example, have been shown to deliver more charge, than smooth, glassy carbon electrodes [37]. In fact, porous carbons are widely used as the electrode materials in electric double-layer capacitors due to their high surface area, good electrical conductivity, and high corrosion resistance [38]. There is a limitation, however, in utilizing the total capacitance of nanoporous electrodes at high charge/discharge rates because the full porosity of the electrodes may not be available [37, 38].

1.4.2. Titanium (Commercially Pure Grade 2)

Titanium is very strong yet weighs about half as much as steel, nickel, and copper alloys. In addition to being strong yet lightweight, titanium has excellent corrosion resistance [39]. Ti has been used as a substrate material for coated electrodes; it has excellent corrosion resistance and biocompatibility in bone tissue, but less blood compatibility in cardiovascular systems [40]. In electrochemical systems, there is a thin TiO_2 layer on the surface, and with electrochemical ageing this layer grows, increasing the electrode's capacitance,

while decreasing its resistance to corrosion [40]. However, this increase in capacitance may not be fully utilized at high frequencies if part of the effective surface area is inaccessible.

1.4.3. Titanium Nitride coated Titanium (Commercially Pure Grade 2)

TiN is used as a surface coating for stimulation electrodes because it is stable under ambient conditions, although some oxidation occurs when exposed to air and oxygen [40]. Grade 2 titanium nitride coated titanium is characterized by overall hardness, heat resistance, oxidation resistance, and lubricity. TiN is also a biocompatible coating that has been approved by the medical industry for years used as the finishing touches to implants and surgical devices [41].

1.4.4. Stainless steel, type 303

Grade 303 stainless steel is the popular name for stainless steel type 1.4305. Grade 303 is the most readily machineable of all the austenitic grades of stainless steel [42]. The machineable nature of grade 303 is due to the presence of Sulphur in the steel composition. Whilst the Sulphur improves machining, it also causes a decrease in the corrosion resistance and a slight lowering of the toughness. The corrosion resistance of type 303 is lower than that for 304, for example. The toughness is still excellent as with other austenitic grades.

In addition to its relatively low corrosion resistance, the presence in its composition of a high quantity of nickel, an agent known to trigger toxic, allergic and cancerogenous responses in humans, is also the cause of some concern [43].

1.4.5. Electrochemical Impedance Spectroscopy (EIS)

Stimulation efficiency is determined by the ability to attain a desired physiological response with minimal damage to the surrounding tissue. For each application, electrical stimulation conditions should be optimized by not only choosing appropriate electrode geometry but also by studying electrode material properties and charge-transfer characteristics at the electrode-electrolyte interface.

Electrodes must be biocompatible to avoid toxic or immune responses in the adjacent tissue or medium, and they should efficiently transfer charge from the electrode material where it is carried by *free electrons* to the medium or tissue

where it is carried by *ions*. Charge transfer can occur through three mechanisms: (i) non-faradaic charging/discharging of the electrochemical double layer, (ii) reversible faradaic reactions, and (iii) non-reversible faradaic reactions [27]. The first two mechanisms are desirable, while the last should be avoided because it is associated with electrode degradation and harmful byproducts. The relative presence of each mechanism can be assessed using electrochemical impedance spectroscopy (EIS), from which an equivalent circuit of the stimulation system can be constructed.

EIS is a general term referring to the measurement of the linear electrical response of a material of interest and the subsequent analysis of the response to yield information about the electrochemical properties of the system [44]. Electrochemical impedance is usually measured by applying an AC potential to the electrochemical system and measuring its current for a range of frequencies. In normal EIS practice, a small (1 to 10 mV) AC signal is applied to the electrochemical system at hand. The signal is small enough to keep the system confined to a pseudo-linear segment of the cell's current versus voltage curve. Moreover, the system being measured should be at a steady state throughout the time required to measure the EIS spectrum, and measuring an EIS spectrum may often take many hours if the range of frequencies under study includes those under 10^{-1} Hz. A small signal reduces the likelihood that the system will drift out of a steady-state condition [45]. For our purposes in this study, we compare the use of several different electrode types for use bioreactors, and these bioreactor may deliver much higher voltages to the cells being cultured (on the order of 1-10 V). By performing EIS measurements with different input voltages, therefore, although the systems themselves are likely not at steady state, we can compare the responses of the different electrodes to different input voltages in order to determine the ease with which the systems drift out of steady state, which is useful for predicting bioreactor performance.

After an EIS measurement is taken, common practices include generating Nyquist and Bode plots, as well as using EIS data to generate equivalent circuit models of the system. The relative presence of faradaic, reversible-faradaic and non-faradaic reactions can then be assessed.

1.4.6. Equivalent Circuit Models for Electrochemical Systems

EIS data is commonly analyzed by fitting it to an equivalent electrical circuit model, which usually includes common circuit elements such as resistors, capacitors, and inductors. When EIS data are fit to equivalent circuit models it can be a very useful tool to help formulate a hypothesis about the processes and mechanisms at work in a given electrochemical system. Often, an equivalent circuit model which fits the data will suggest some chemical model, process, or mechanism which can be proposed and tested. In order to provide insight into the behavior of the system being analyzed, the elements in the model should have a basis in the physical electrochemistry of the system.

In **Figure 2**, for example, which shows the equivalent circuit for a simple electrochemical cell, Rs represents the resistance of the bulk solution, Rp represents the polarization resistance, which also represents the electrode's resistance to corrosion, and $C_{double\text{-}layer}$ represents the capacitance of the double layer of charge induced by the accumulation of electrons on the electrode and the corresponding accumulation of ions in the solution in proximity to the electrode.

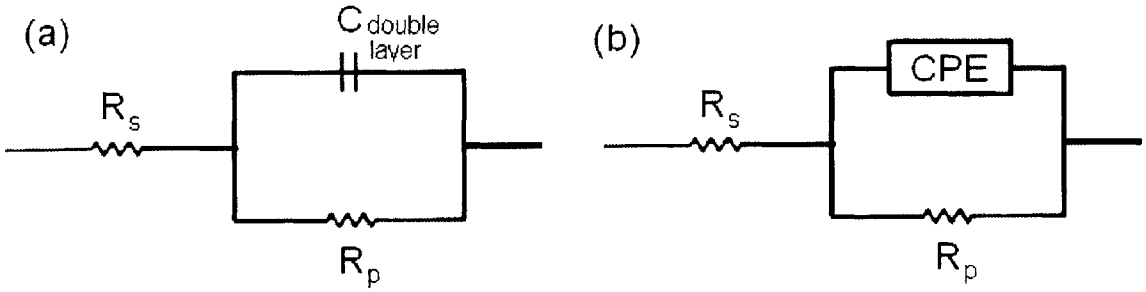

Figure 2: (a) The equivalent circuit of a simple electrochemical "Randles" cell, where Rs represents the solution's resistance, $C_{double\ layer}$, the double layer capacitance, and Rp the polarization resistance. (b) The equivalent circuit of a simple electrochemical cell with a CPE instead of a double-layer capacitance. This equivalent circuit is generally a more accurate description of electrochemical systems.

The impedance modulus Z of an electrochemical system as depicted in **Figure 2(a)** can be expressed as a function of frequency:

$$Z(j\omega) = R_s + \frac{R_p}{1 + j\omega C_{dl} R_p} \qquad \text{(Eq. 1.4.6.1)}$$

in which Rs, otherwise known as the solution resistance, represents the high-frequency limit of the impedance, and Rs + Rp represents the low-frequency limit of the impedance, where Rp is the resistance to a polarization, or corrosive, current, inversely proportional to the corrosive current density [46].

The resistance of an ionic solution depends on the ionic concentration, type of ions, temperature and the geometry of the area in which current is carried, and its theoretical value is given by:

$$R_s = \frac{l}{\sigma A} \qquad \text{(Eq. 1.4.6.2)}$$

Where Rs is resistance (in Ohms), l is the distance between the electrodes carrying a uniform current (in meters), σ is the conductivity of the ionic solution (in S/m) and A is the area of the electrodes (in m^2) [45].

Whenever electrodes are forced away from their equilibrium potential, current may flow due to reactions on the surfaces of the electrodes or charge accumulation on the surfaces of the electrodes. The polarization resistance refers to the ease with which current is made to flow—the lower its value, generally, the higher the rate of corrosion [45].

A so-called electrical double layer exists at the interface between an electrode and its surrounding electrolyte. It is formed in response to the positive or negative electric charge of the electrode as cations and anions accumulate, respectively, at the solution side of the charged electrode, and its thickness of is on the order of 0.3-0.5 nm [47]. The value of the double layer capacitance depends on many variables including electrode potential, temperature, ionic concentrations, types of ions, oxide layers, electrode roughness, impurity adsorption, etc. [45]. Due to non-homogeneities in electrochemical systems, a so-called "constant-phase element" (CPE) is used in a circuit model in lieu of a capacitor [45, 48]. An ideal capacitor is actually a constant phase element with a constant phase angle of 90 degrees, but a CPE may have any phase angle value.

The impedance Z of a capacitor can be expressed as:

$$Z = \frac{(j\omega)^{-\eta}}{C} \qquad \text{(Eq. 1.4.6.3)}$$

where j is the imaginary number, ω is the angular frequency in radians, C is the capacitance of the electrochemical cell in farads, and η is an exponent expressing the degree of non-ideality of the CPE, and ranges in value from 0 to 1. For an ideal capacitor, η is equal to 1, but for constant phase element, the exponent η is less than one. The "double layer capacitor" on real cells often behaves like a CPE, not a capacitor [45], and this empirical factor may correspond, in the case of a corroding metal, to surface roughening [46], or other factors including non-uniformities of reaction rates, coating thicknesses, or current distributions [49].

When examining EIS data, common practices include generating Nyquist and Bode plots, because the shapes of the curves facilitate insight into the mechanisms governing the behavior of the electrochemical system to the trained eye. In **Figure 3,** for example, we can see from the Nyquist plot of a theoretical electrochemical system that, all other parameters being equal, with decreasing Rp values, the Nyquist plot looks more and more "semi-circular." In a corresponding fashion, the Bode plots of the same system appear less and less like that of an ideal capacitor with decreasing Rp values.

In **Figure** 4, for example, we can see from the Nyquist plot of a theoretical electrochemical system that, all other parameters being equal, with increasing η values, the Nyquist plot looks more and more "semi-circular." In a corresponding fashion, the Bode plots of the same system appear less and less like that of an ideal capacitor with decreasing η values.

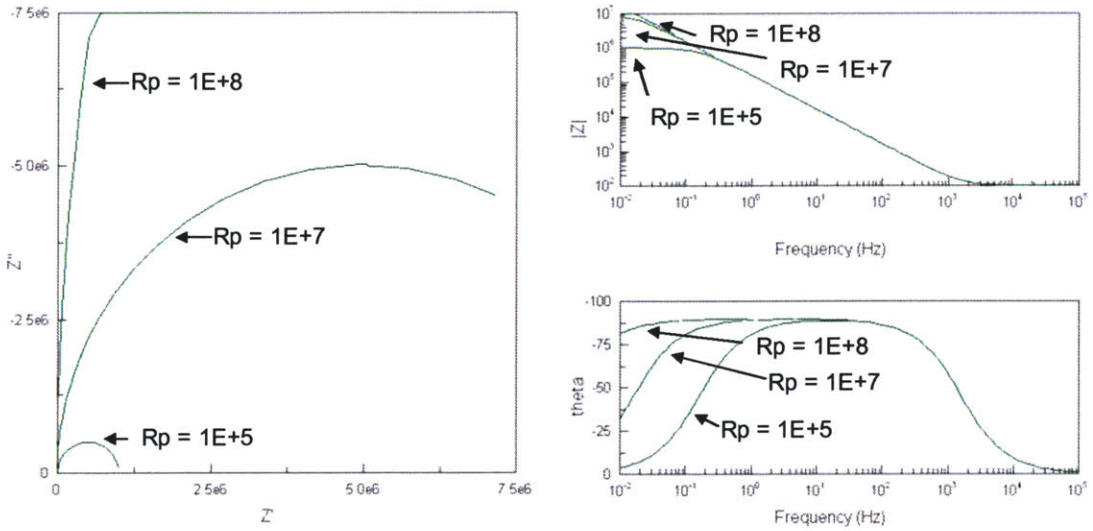

Figure 3: Nyquist and Bode plots for circuit models of Randles cells of Rs = 100Ω, C_{dl} = 1μF, η=1, and increasing values of Rp (and therefore corrosive reactions). As the value for Rs increases, the Nyquist plot looks less and less semi-circular, and the Bode plot looks less and less like that of an ideal capacitor.

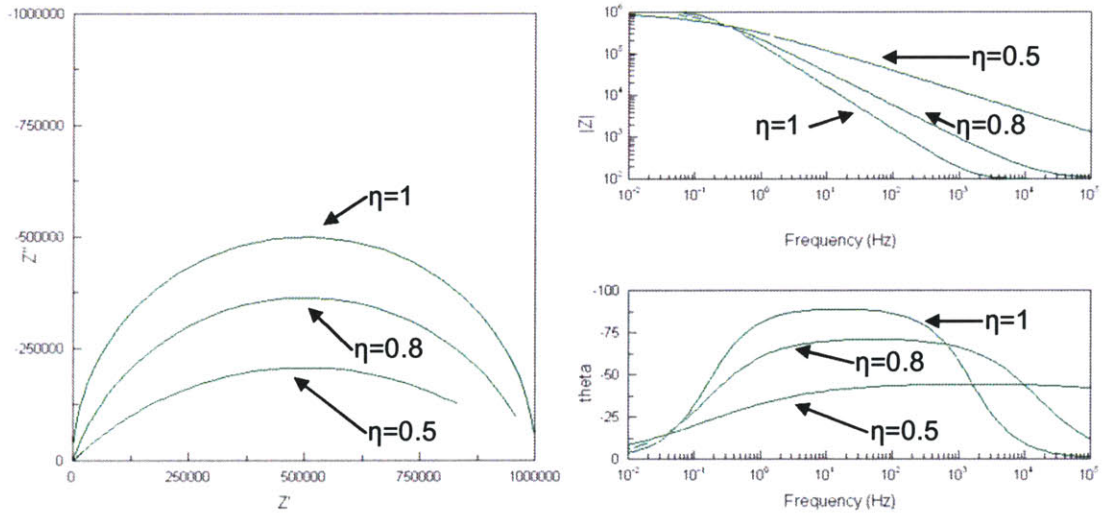

Figure 4: Nyquist and Bode plots for circuit models of Randles cells of Rs = 100Ω, C_{dl} = 1μF, Rp=1E+6 Ω and increasing values of **η**. As the value for **η** increases, the Nyquist plot looks more and more semi-circular, and the Bode plot looks more and more like that of an ideal capacitor.

2. MATERIALS AND METHODS

Ever since Galen, the second century Greek physician believed to be the father of western experimental physiology, conducted his anatomical research on animals, extrapolating his results to humans and initiating many errors, the experimentation on animals has become an essential part of biomedical research, but with the caveat of whether results from animal studies can be extended to humans [50]. In terms of cardiac tissue engineering, the topic of cell source and animal model has been the topic of much discussion. In order to test prospective tissue-engineered devices, constructs must first be proven in animal models before receiving CE marking or FDA approval for a clinical trial. The choice of animal depends on the nature of the tissue-engineered construct being tested. Factors that need to be considered include technical requirements of implanting the construct, availability of the animal, cost and ethical considerations.

Rats have the advantages of being inexpensive, easy to handle and anaesthetise, and have a variety of strains including those with specific atherosclerotic risk factors like hypertension. However, when it comes to performing surgery their small size presents quite a technical challenge. Hence, compared to other fields of research, they are not as popular as animal models, especially for blood vessel research. However, as discussed above, the rat has proven very useful when studying cardiac muscle tissue engineering and for testing cardiac tissue grafts and as tools to assess the degree of vascularization of tissue-engineered constructs after implantation [50].

By working with neonatal rat cardiomyocytes, I will have the opportunity to build upon previous results demonstrating that co-culturing of neonatal cardiomyocytes, fibroblasts and collagen within bioreactors can produce constructs that show promise for the repair of larger scar areas of the myocardium [50]. For certain preliminary tests, however, it may not be appropriate to use primary cells, and to use cells derived from immortal cell lines instead.

I chose C2C12 mouse myoblast cells as another model system due to their availability, ease of handling, well-described characterization in literature and the

evidence that they differentiate and express cardiac specific proteins when grafted into the rat or mouse myocardium [51-53]. They can be frozen for long periods of time, are immortal, and moreover, they are representative of hypoxia sensitive cells such as cardiomyocytes.

The methodology adopted for this project is therefore to:

(1) Prepare cells from either frozen cell stock or isolated from primary cell sources
(2) Seed cells onto collagen scaffolds using Matrigel®
(3) Stimulate cells with electric field stimulation
(4) Perform assessments

An overview of the experimental setup is shown in **Figure 5**. Seeded scaffolds populated either by rat cardiomyocytes or C2C12 cells are stimulated within bioreactors, which are connected to a computer via an amplifier circuit. The stimulus may be modified by either modifying the geometry of the bioreactors, or by modulating the stimulus as delivered by the computer software.

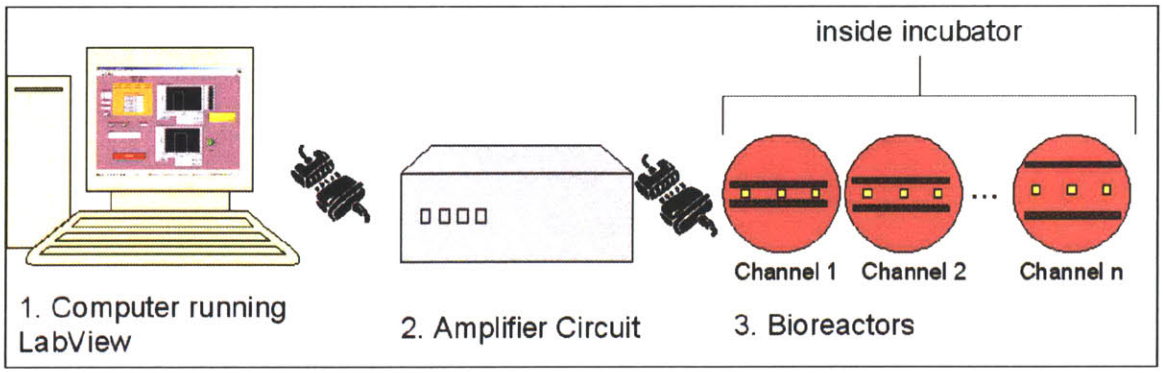

Figure 5: Overview of experimental setup. A computer running custom software generates the pulse shapes which are then reproduced with more power by the amplifier circuit, and then connected via wires to the bioreactors located inside an incubator maintained at 37° C.

2.1. CELL PREPARATION

2.1.1. Isolation of neonatal rat cardiomyocyte cells

Neonatal rat cardiomyocytes are the most frequently used cells in cardiac tissue engineering and I have chosen to use them in this study in order to capitalize on past studies. We obtained cardiomyocytes from 2-day old neonatal Sprague Dawley rats, using a protocol approved by our Committee on Animal Care.

We first excise hearts from neonatal rat pups, and then remove the right and left atria, in addition to any remaining blood vessels, from the rest of the heart. Atria and blood vessels protruding from the superior portion of the heart are removed because atrial natiuretic factor (ANF) is produced only in the atria under basal conditions. In addition, we remove any smooth muscle cells and endothelial cells in the major blood vessels from the preparation in order to reduce the number of variables in the experiment, although co-culture conditions with endothelial cells may be included in future work.

We then cut tissue samples into four pieces and subject them to an overnight trypsin digestion at 4°C, while agitating at a rate of approximately 50 oscillations per minute. The next day, we halt the trypsin reaction by adding high-serum (10% FBS) medium to the tissues and agitating for 4 minutes. In progressive steps, we remove the supernatant containing cells from the rest of the tissue and subject the remaining pieces of tissue to another collagenase digestion.

After all the pieces of tissue have been digested, we spin the cell solution in a centrifuge at low speed (500rpm) for 10 minutes, as a first step toward separating the myocytes from the non-myocytes, since the myocytes will pellet at the bottom of the tube and other cell types will tend to remain in the supernatant at this speed. Next, we resuspend the pellet and centrifuge again at 700rpm in order to increase the purity of the sample. Next, we resuspend the pellet again in an appropriate amount of culture medium comprised of DMEM with 10% FBS, 1% HEPES and 1%Pen-strep and we distribute the mixture into tissue culture flasks, which are incubated in a humidified chamber for 75 minutes at 37°C and 5% CO_2 in order to further purify the sample of rat ventricular myocytes from other cell types, mainly fibroblasts, since fibroblasts and other non-myocytes tend to plate much earlier than the myocytes, and so the remaining suspension in the flask will ideally be enriched in concentration of rat ventricular myocytes. Finally, we pellet

and resuspend the rat cardiomyocyte cells in Matrigel® in order to be seeded onto scaffolds.

Because the isolation of the neonatal rat cardiomyocyte cells is comprised of many steps involving much handling, there are many potential complications that may arise during this process. Maintaining sterility is of the utmost importance, but time is also of the essence, and so good techniques must be developed that sacrifice neither sterility nor time. In addition, removing trypsin and collagenase from the cells while not eliminating any cells is a crucial step in the experiment, as the presence of either of these enzymes will either prevent tissue formation, or maintenance of the scaffold, respectively. Limiting the number of pups used in any given isolation procedure to 20 is helpful to minimize any of the above complications. In addition techniques employed for isolation of rat cardiomyocytes must also be consistent from experiment to experiment in order to reduce variations.

2.1.2. Preparation of C2C12 mouse myoblast cells

Conversion of mouse C2C12 myoblasts into myotubular structures represents a well-established and robust *in vitro* differentiation model [54]. Proliferating myoblasts can be induced to differentiate into myotubes by growing them to confluence and switching them to reduced serum medium. Under these conditions, most cells fuse to form myotubes after 4 days [54]. In this study, C2C12 cells are therefore expanded and stimulated under different serum-content medium conditions. For expansion of the cells, we expand C2C12 cells (after being thawed from frozen cell stock stored under liquid nitrogen in a cryostat in 5% Dimethylsulfoxide (DMSO) solution) in growth medium comprised of Dulbecco's Modified Eagle Medium (DMEM) with N-2-Hydroxyethylpiperazine-N'-2-Ethane-Sulfonic Acid (HEPES), 10% fetal bovine serum (FBS) and 1% Penicillin/Streptomycin (Pen-strep). When cells are about 80% confluent, I then wash the cells in a 1x phosphate-buffered saline solution (PBS), trypsinize them, and either expand or seed them onto Ultrafoam® collagen scaffolds (6x8x1.5mm) using Matrigel® at a concentration of 200,000 cells/μL and 5 million cells/scaffold. If cells are to be seeded at this point, we switch the serum content to fusion medium with a reduced (2%) FBS content in order to induce differentiation. Otherwise, we maintain them in growth medium.

2.1.3. Scaffold Preparation and Seeding

Once we have prepared the cells for seeding, we then resuspend the cells in Matrigel® at a concentration of 200,000 cells/μL. We keep both the Matrigel® and cells on ice during this step. We selected Matrigel®, a basement membrane preparation extracted from the Engelbreth-Holm-Swarm mouse sarcoma and solubilized in DMEM at the concentration of 7.458 mg/ml, for this study because it contains laminin and collagen IV known to promote surface attachment of cardiac myocytes [5]. Gel inoculation has also been found to satisfy the requirements of uniform seeding density with high seeding yield that maximizes donor cell utilization, an essential feature for cells with limited proliferation potential, such as cardiomyocytes [6]. We resuspend cells at this concentration while working on ice to prevent premature gelation (Matrigel® is a liquid at 2-8°C and it gels rapidly at 22-35°C). Scaffolds were rectangles or squares with dry dimensions of 6x8x1.5mm or 6x6x1.5mm, respectively, cut from sheets of Ultrafoam® collagen hemostat (Davol Inc., Cranston, RI), a water-soluble, partial HCl salt of purified bovine dermal (corium) collagen formed as a sponge with interconnected pores. The use of collagen as a 3-D matrix support is consistent with its role in normal muscle [55]. Furthermore, there is evidence that stimulation of extracellular matrix production around individual myotubes is enhanced by the presence of pre-existing extracellular matrix [56].

We gently blot-dry pre-wetted scaffolds and the Matrigel®/cell suspension is then delivered quickly and evenly to the top surface of each scaffold using a micro pipette. Gelation is typically achieved within 10 minutes of the transfer, but the scaffolds are allowed to settle for 20 minutes before they are handled again. After this 20 minute period, we preculture the cells on the scaffolds for 3 days in 4mL of culture medium (fusion medium for C2C12 cells) in a 37°C/5% CO_2 humidified incubator to allow the cells to attach to the scaffolds and recover from isolation.

2.2. BIOREACTOR ASSEMBLY

To assess cell alignment after stimulation, it is desirable to maintain a constant alignment of scaffolds with respect to the direction of the electric field gradient, while at the same time not restricting the contractions of the tissue construct nor the ability to observe the constructs with a microscope. For this study, we

accomplish this task using stainless-steel pins, held in place by a thin layer of PDMS at the bottom of a Petri dish (see **Figure 6**Error! Reference source not found.). For a discussion of the design of this bioreactor, see **Section 3.2.1**).

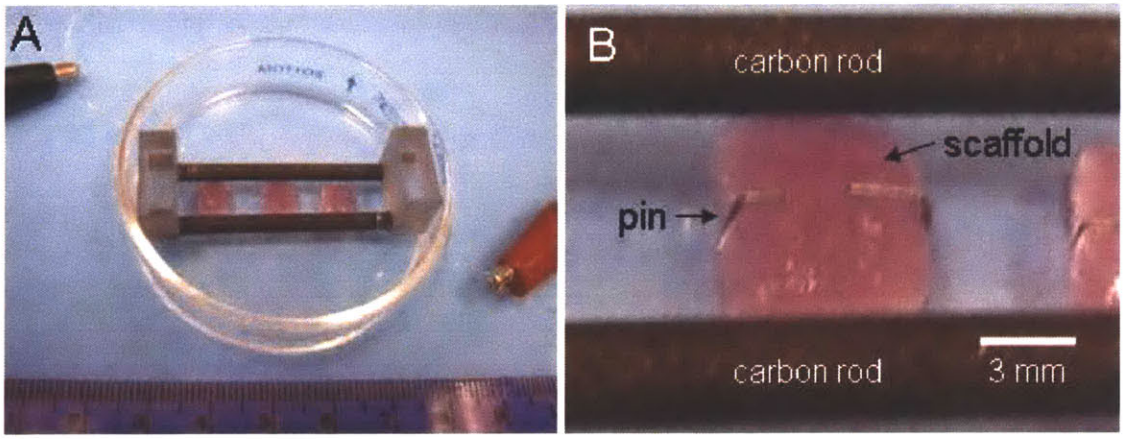

Figure 6: Assembled bioreactor. A. 60 mm Petri dish with carbon rod electrodes, spaced 1 cm apart. B. Close up view of scaffold positioned between electrodes and held in place with two stainless steel pins.

2.3. ELECTRICAL CHARACTERIZATION OF BIOREACTOR

Stimulation efficiency is determined by the ability to attain a desired physiological response with minimal damage to the surrounding tissue. For each application, electrical stimulation conditions should be optimized by not only choosing appropriate electrode geometry but also by studying electrode material properties and charge-transfer characteristics at the electrode-electrolyte interface. Electrodes must be biocompatible to avoid toxic or immune responses in the adjacent tissue or medium, and they should efficiently transfer charge from the electrode material to the medium or tissue. Electrochemical impedance spectroscopy (EIS) allows us to assess the relative presence of non-faradaic charging/discharging of the electrochemical double layer, reversible faradaic reactions, and non-reversible faradaic reactions, and to create an equivalent circuit of the stimulation system. This information permits us to assess the tradeoffs for each electrode between improved charge injection and creation of harmful reaction products.

2.3.1. EIS Measurements of Bioreactor

For this study, we have taken EIS measurements with an electrochemical interface (Solartron 1287) and a frequency response analyzer (FRA, Solartron 1250) controlled by a computer with ZPlot software. We have calculated the values for equivalent circuits and associated parameters using the instant fit and manual fit functions in ZView 2.5b software. In this software, element errors are calculated by testing several solutions with the weighted sum of squares method near the 'best fit,' and determining the range until the goodness of fit starts to decrease. If 98 and 102 Ohms produces a very similar goodness of fit, for example, but 97 and 103 Ohms produces a poorer fit, the error is reported as 2 Ohms [57].

We have made measurements in PBS to facilitate comparison with EIS data in the literature and from our own laboratory. The conductivity of PBS (15 mS/cm) is similar to that of culture medium with 10% FBS (~14 mS/cm). Please see [37] for additional information on EIS measurement of common electrode materials.

2.3.2. Current Measurement in the Bioreactor

The amount of injected charge is calculated simply by measuring the potential drop across a resistor placed in series in the stimulation loop, and then using Ohm's law to back-calculate the current, by dividing this measured voltage by the value of the resistor. In order to calculate injected charge, the current is integrated over time using SigmaPlot software during a single stimulus. Immediately after the application of a stimulus, the current in the bioreactor setup reverses direction, and the amount of current during this recovery period is a function of the reversibility of the mechanisms of charge injection. In order to determine the amount of charge which remains unrecovered after the application of a stimulus, the current is integrated until the current flowing in the bioreactor reaches a steady state.

2.3.3. Choice of the Electrode Material

The design considerations required for electrical stimulation of engineered cardiac tissue are many and interdependent. Factors to consider include the duration and shape of the stimulus waveform, the size of the tissue construct in

question, the electrical property being exploited (generation of reactive oxygen species versus eliciting action potential, for example), the duration of the experiment, and the mechanical properties required of the electrode in the bioreactor setup. For this study we started with a desired stimulus waveform, examined the electrical characteristics of that stimulus, and based subsequent design decisions with this in mind. Waveform selection (e.g., between monophasic, biphasic or other wave shapes) depends on the electrode material characteristics, as biphasic pulses can aid in reversing reversible faradaic reactions, but at the same time may be undesirable since biphasic pulses may inhibit action potential.

2.4. ELECTRICAL SIMULATION OF CONSTRUCTS

The objective of electrical stimulation is to deliver enough current to cells to depolarize membrane and elicit an action potential. In addition, there is some evidence that electrical stimulation aids in cardiomyocyte alignment. For scaffolds of cardiomyocytes seeded with Matrigel® it has been previously determined that the optimal time to begin electric field stimulation is 3 days after scaffolds are seeded and to assess contractile function after 8 days [5]. Electric field stimulation may be delivered from a commercially-available stimulator or through custom-designed hardware controlled by a computer. Although computer-controlled stimulation allows additional flexibility, it requires some expertise in circuit design and software programming.

We chose monophasic pulses for their simplicity, and because the reversal of faradaic reactions that biphasic pulses would allow is unnecessary with carbon electrodes, which exhibit a high resistance to reactions. In addition, by choosing monophasic pulses, we also avoid the undesirable effect of biphasic pulses inhibiting action potentials (see **Section 2.3.3** for details).

2.5. ASSESSMENTS

The progression of tissue assembly can be assessed at various hierarchical levels. At the functional level, the amplitude of contractions, excitation threshold, maximum capture rate and transmembrane potentials can all be measured, and at the ultrastructural level, morphology of cells and nuclei, development and

volume fraction of sarcomeres, and the development and frequency of sarcomeres, and the development and frequency of gap junctions, intercalated disks, mitochondria, and microtubules, may be observed [5].

Functional gap junctions, cytoskeletal organization, and excitation-contraction coupling are all necessary for the development of contractile behavior. From a clinical perspective, monitoring outputs related to clinical functional aspects are important. From a biological aspect, and for research purposes, however, investigating biological pathways is valuable in order to improve our knowledge of the mechanisms of cardiac differentiation. The approach undertaken in this study is therefore to assess constructs at the functional level first, since this behavior represents a minimum functional requirement of a cardiac patch and sporadic contractions are normally exhibited even under control conditions. Moreover, assessments at the molecular and ultrastructural levels are destructive, expensive and time-consuming in nature. After we perform functional analysis to determine an appropriate range of stimuli, therefore, we conduct more detailed experiments incorporating further investigation at the molecular and ultrastructural levels. Preliminary results indicate that a range between 0-10V/cm is appropriate for 2mS wide pulses at a 1Hz stimulation rate (see **Section 3.3.1** for a discussion of stimulation levels).

2.5.1. Contractile Activity

With no electrical stimulation, neonatal rat cardiomyocytes seeded onto collagen scaffolds with Matrigel® will often contract spontaneously, although in culture, the cardiomyocyte generally loses this phenotype [58]. Perhaps this spontaneous electrical activity is due to the presence of pacemaker cardiomyocytes in the preparation (see **Section 1.1.1** for a description of types of cardiomyocytes), but in any event, a logical functional assessment is therefore to compare the contractile properties of the engineered tissue with those of the control, which itself does contract.

One measurement that has been used in the past of the electrical excitability of engineered tissue is a comparison of the threshold voltage required to induce visible contraction at a rate of 1 beat/second [5]. A potential problem of any method relying on human observance is an inherent subjectivity, but with

healthier cultured constructs this threshold voltage is quite defined and so easier to observe, and so may not be a problem with good experimental techniques for seeding scaffolds. Another set of potential problems is related to the variability of the performance of the engineered constructs due to cell fatigue during determination of threshold voltage, adaptation of electrically excitable cells to electrical stimulation (a decline in the response of electrically excitable cells to maintained stimuli), as well as fluctuations of environmental conditions such as temperature, humidity and gas composition from laboratory and incubator conditions. Cardiomyocyte beat rate has been shown to closely follow temperature and pH profiles, for example [59, 60], and both of these factors change dramatically at ambient room and incubator conditions. We therefore employ a temperature controller attached to a thermocouple in this study to keep the temperature of the constructs at 37°C.

We evaluate contractile function of engineered cardiac constructs on-line (during culture) by measuring contractile activity in response to electrical field stimulation. Once we determine the threshold excitation voltage, this value is multiplied by 1.5 and we apply this voltage while varying the excitation frequency, in order to determine the maximum rate at which the construct can be paced, a measure of cell health and electrical excitability in the construct. .

2.5.2. Histological Analysis

In order to perform histological analysis on the cell-scaffold constructs, we first fix them in a 10% buffered formalin for 24 hours, before they are dehydrated, embeded in paraffin, bisected in cross section through the center, and sectioned to 5 μm thickness. Sections are then stained with hematoxylin and eosin for general evaluation and stained with cardiac specific antibodies to assess the distribution of cardiac markers. We have used a humidified chamber for all incubation steps.

2.5.3. Ultrastructure Analysis

One challenge of 3-D tissue engineering is the performance of ultrastructural analysis using microscopy. In order to perform traditional wide-field microscopy, for example, samples must be fixed and then sectioned before any images may

be taken. Not only is this a time-consuming process, but the sectioning process itself may separate pieces which would then need to be reassembled later for 3-D reconstruction and subsequent analysis. Confocal microscopy has the advantage of providing clear optical slices for visualization of samples, but has the disadvantages of being time-consuming and expensive. A disadvantage, however, is that the procurement of any confocal images must be performed relatively quickly (within a few days) after the end of an experiment because samples can not be mounted on slides. Nonetheless, for this study, I have immunostained samples and visualized them using confocal microscopy, as it has proven to be the best method for visualization of the 3-D samples in question.

3. RESULTS AND DISCUSSION

Design of efficacious and safe electrical stimulation should allow minimal damage to both surrounding tissue and electrode. Design factors to consider include the choice of electrode material, electrode geometry and real area, waveform type and stimulation frequency.

3.1. ELECTRODE CHARACTERIZATION

3.1.1. Surface properties of electrodes

The electrode material chosen for an electrical stimulation application should exhibit high charge storage capacity, therefore allowing more charge to be injected before the onset of Faradaic reactions. Storage capacity is a factor not only of material properties, but also of electrode geometry and real area (including roughness).

Figure 7 shows a comparison of scanning electron microscope (SEM) images obtained for porous carbon, stainless steel, titanium and titanium nitride-coated titanium at 30x and 1000x magnification. At the 30x magnification, a marked difference in surface texture is evident among the electrodes: carbon appears obviously rougher than any of its counterparts, and stainless steel appears the smoothest. At the 1000x magnification, the difference in surface texture of the carbon, titanium nitride and titanium is less evident, although the surface topography of the stainless steel still appears to be composed more of ridges than pores.

This ranking of the electrodes in terms of their surface roughness via SEM is not rigorous, but serves as an indication of the surface characteristics of the electrodes at hand. Indeed, for a detailed study of the surface characteristics of the electrodes, atomic force microscopy (AFM) would be a more ideal choice, as it provides extraordinary topographic contrast, and allows for direct height measurements and unobscured views of surface features without the use of coatings. Nonetheless, SEM images are obtained faster and give a good sense of the microstructure of the electrodes.

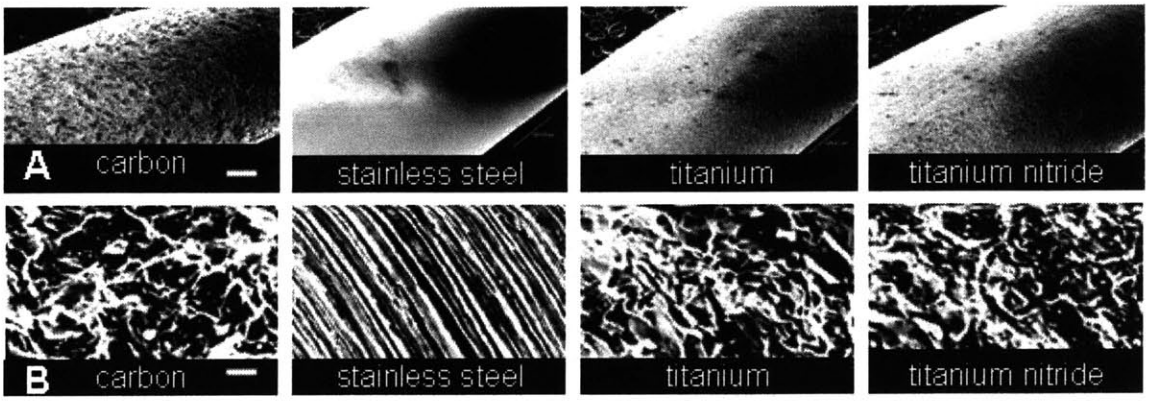

Figure 7: (a) 30x scanning electron microscopy (SEM) images of electrodes, 1/8" diameter. White bar corresponds to 500 μm. Higher surface porosity contributes to higher levels of current injection. (b) At 1000x magnification the difference in porosity of carbon versus titanium and titanium nitride is less obvious, implicating the importance of other factors including electrode surface nanostructures, and chemical and material properties for explaining charge storage capacity differences among carbon, titanium and titanium nitride. Stainless steel, however, still has no visible pores at this magnification. White bar corresponds to 10μm.

As stated in **Section 1.4.6**, the value of the double layer capacitance of an electrode depends on many variables besides the electrode's surface roughness. The value of performing EIS measurements can therefore not be underestimated.

3.1.2. Electrode material

Figure 8 shows a comparison of EIS data for the four different electrode materials under study. The semicircular shape for stainless steel in the Nyquist plot suggests a low enough value of Rp to allow for reactions (see **Section 1.4.6** for a discussion of the interpretation Nyquist plots), whereas titanium, titanium nitride, and carbon have progressively more linear profiles associated with high polarization resistance. Moreover, the impedance modulus |Z| is lower at all frequencies for carbon in comparison to the other electrodes, suggesting a higher charge injection capability. The spectra of all samples exhibit one time constant feature, and so the simple equivalent circuit described in **Section 1.4.6** is sufficient for modeling the electrode/electrolyte interfaces, and will be used for all subsequent analyses.

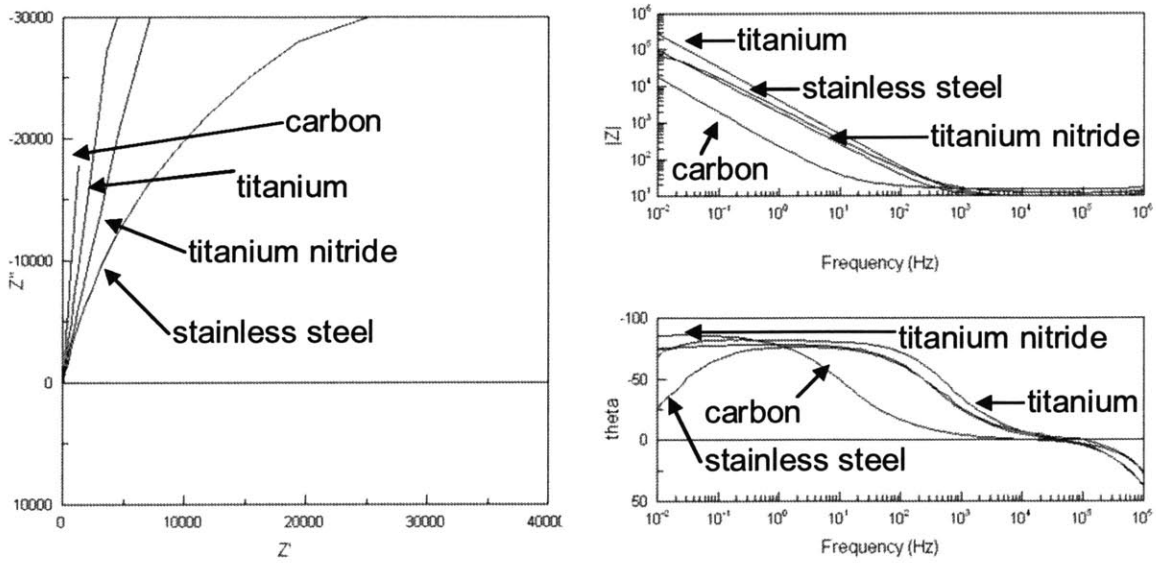

Figure 8: Nyquist and Bode plots comparing 4cm long electrodes of different materials, placed 1cm apart. The semicircular shape of stainless steel in the Nyquist plot (B) suggests the presence of reactions, whereas titanium, titanium nitride, and carbon have progressively more linear profiles associated with high polarization resistance.

3.1.3. Electrode geometry

Electrochemical systems are in general not linear systems, and so insight into the forces at work is often gained by analyzing EIS measurements, to understand the relative importance of factors including geometry, surface roughness, level of electrical stimulation etc.

Figure 9, for example, shows the theoretical value of solution resistance calculated based on Equation 1.4.6.2, along with the values obtained for some corresponding geometries of carbon electrodes. The values measured for increasing distances between the electrodes appear to exhibit a linear relationship, as would be expected by theory, but the theoretical values overestimate the resistance of the system. The theoretical and measured values for increasing lengths of electrodes likewise exhibit the same hyperbolic relationship, but again with the theoretical values overestimating the measured values. Possible sources of this discrepancy include equipment calibration and underestimation of "real" electrode area due to surface roughness. Nonetheless, the theoretical relationship between electrode geometry and solution resistance allows us to make predictions about the effect on the electrochemical behavior of the system at hand, and aids in bioreactor design.

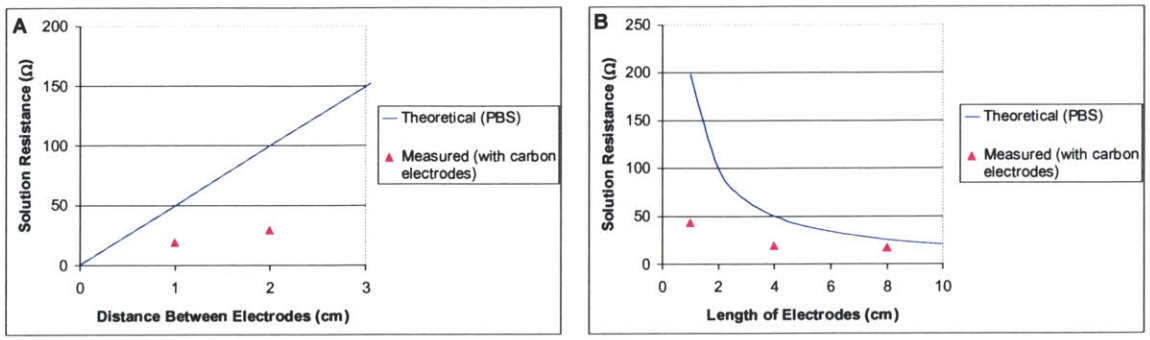

Figure 9: Calculated theoretical solution resistance for different geometries of PBS and measured solution resistance in electrochemical systems of corresponding geometries comprised of carbon electrodes for (A) electrodes of 4 cm length and increasing distances, and (B) electrodes placed 1 cm apart and of increasing lengths.

Figure 10 shows Nyquist and Bode plots for electrodes with equal spacing between them, but of different lengths of porous carbon. For porous carbon electrodes, the main difference between the electrochemical characteristics of systems composed of equally-spaced yet increasingly long electrodes is the observed decrease in electrolyte resistance, Rs, which is evident in the change of the value of the high-frequency value of the impedance modulus |Z|. This decrease corresponds directly to the increased volume of electrolyte located between the electrodes. CPE, Rp and η values remain equivalent.

Since the slope of the Nyquist plot is so high for all three electrode geometries, we expect the calculated values for Rp to be very high. In fact these values are so high that they approach the limit at which they can be calculated with this bandwidth.

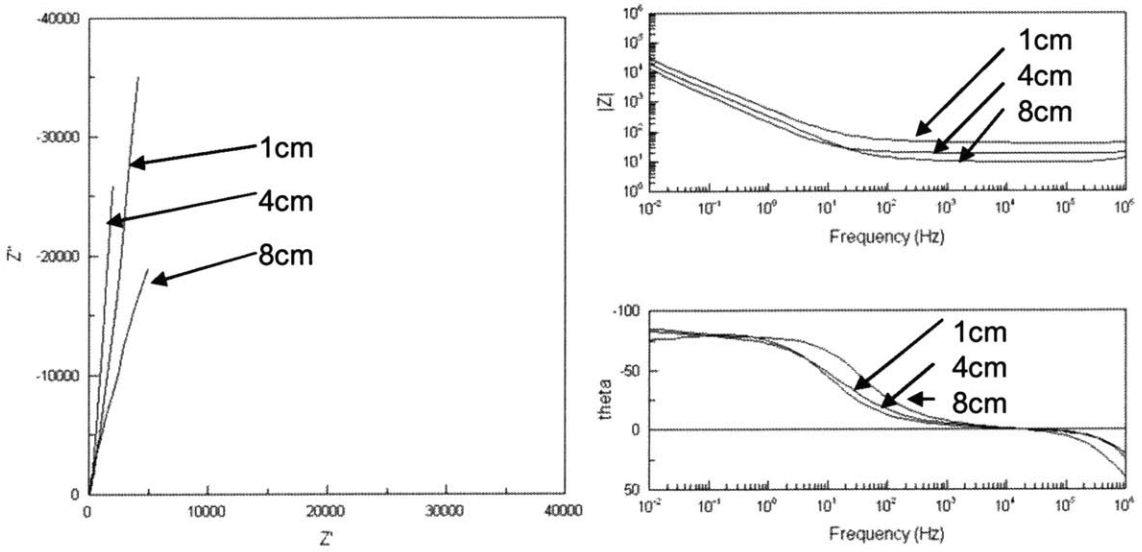

Figure 10: Nyquist and Bode plots of carbon rod electrodes spaced 1 cm apart, and of different lengths, in PBS. The main value to change for the electrode configurations is the value of Rs, the high-frequency value of |Z| on the Bode plot.

Table 1 lists a summary of calculated equivalent circuit parameters for different electrode geometries for carbon, stainless steel, titanium nitride and titanium. In terms of bioreactor design implications, it is worth noting that although changes in the length or spacing of electrodes may not contribute very strongly to observable differences in EIS measurements or certain equivalent circuit parameters for carbon, the delivered stimulus, from the stimulated cell's perspective, however, will differ in terms of the absolute amount of reaction products created in the culture medium. The electrode geometry employed should therefore minimize the amount of exposed electrode surface area while retaining tolerable Rp and CPE values. The tolerable values for these parameters will be determined on an individual basis by the bioreactor at hand and the stimulus waveform applied to the cells. A short stimulus waveform for example, may weigh in favor of improving charge injection despite the creation of increasing amount of reaction products.

The overall decreased value of Rp for stainless steel, titanium nitride, and titanium, in comparison to carbon implies that reaction products are much more of a risk. The increased sensitivity of the EIS measurements to geometry, however, for these materials, is notable, and so, in terms of design, the tradeoff between exposed surface area and charge injection capabilities will be much more pronounced.

Electrode Length (cm)	Electrode Spacing (cm)	Rs, Ω (% error)	CPE/cm² (% error)	R_p Ω/cm² (% error)	η (% error)
Carbon					
1	1	42.92 (0.99%)	3.6E-4 (1.0%)	9.81E+13 (0.12%)	0.84 (0.41%)
1	2	64.56 (1.54%)	4.31E-4 (1.7%)	3.97E+13 (0.58%)	0.82 (0.71%)
4	1	18.89 (0.93%)	9.07E-4 (0.90%)	5.59E+14 (0.02%)	0.91 (0.28%)
4	2	29.06 (0.80%)	9.05E-4 (0.93%)	1.65E+13 (0.34%)	0.89 (0.38%)
8	1	10.1 (1.85%)	5.9E-4 (0.74%)	1.10E+14 (0.04%)	0.88 (0.23%)
8	2	17.12 (0.51%)	6.08E-4 (0.51%)	1.35E+14 (0.02%)	0.85 (0.18%)
Stainless Steel					
2	1	32.65 (2.03%)	1.36E-4 (2.63%)	2.01E+4 (4.85%)	0.70 (0.82%)
4	1	18.47 (3.97%)	1.75E-4 (4.54%)	2.5E+4 (0.02%)	0.73 (1.31%)
8	1	11.54 (2.64%)	4.9E-4 (3.37%)	7.5E+3 (0.04%)	0.73 (1.09%)
Titanium Nitride					
2	1	34.07 (1.69%)	1.17E-4 (1.78%)	1.85E+5 (13.33%)	0.84 (0.60%)
4	1	19.53 (1.23%)	3.64E-4 (2.66%)	6.76E+3 (12.06%)	0.76 (0.85%)
8	1	10.34 (1.43%)	2.08E-4 (1.34%)	2.29E+5 (22.91%)	0.82 (0.41%)
Titanium					
2	1	32.65 (2.03%)	1.36E-4 (2.63%)	2.01E+4 (4.85%)	0.70 (0.82%)
4	1	18.28 (1.82%)	8.60E-5 (1.77%)	8.44E+4 (5.59%)	0.76 (0.52%)
8	1	11.55 (1.95%)	9.22E-5 (1.69%)	1.72E+5 (9.69%)	0.82 (0.47%)

Table 1: Summary of equivalent circuit parameters for electrodes of different materials, lengths and spacings, measured at 10 mV perturbation. With increasing electrode spacing, the value of the electrolyte resistance Rs generally increases, the value for Rp remains constant, and the value for η decreases. For increasing electrode lengths, CPE generally increases, Rp and η remain constant, and Rs decreases. With increasing electrode lengths, more reaction products will be created on an absolute basis with equal applied stimuli.

3.1.4. Electrode ageing

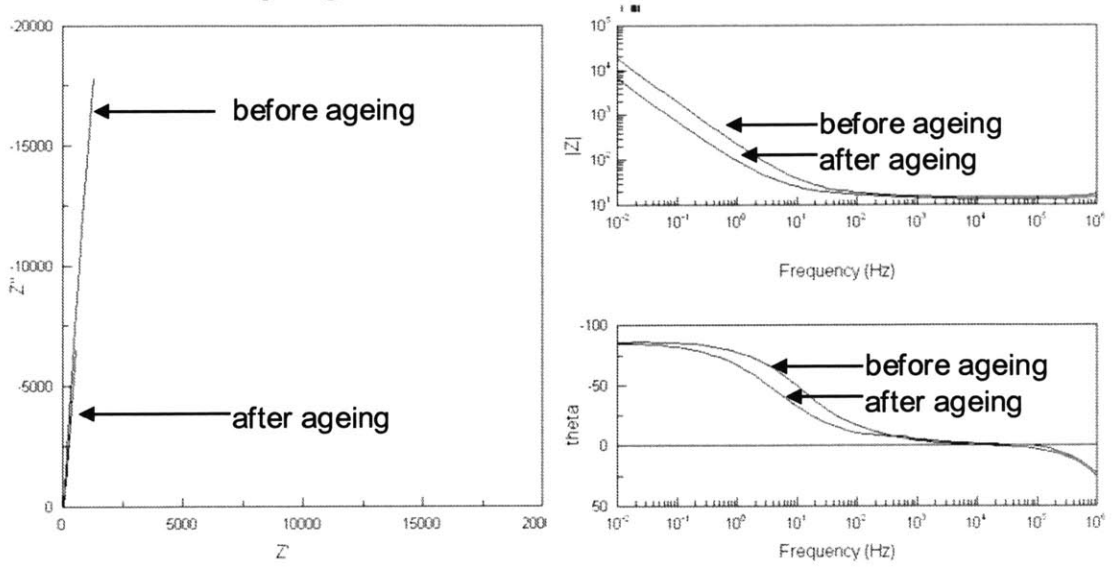

Age	Rs, Ω (% error)	CPE/cm² (% error)	R_p Ω/cm² (% error)	η (% error)
New	16.15 (1.38%)	7.68E-4 (1.67%)	3.59E+13 (0.18%)	0.91 (0.60%)
After 1 experiment	14.90 (1.47%)	2.0E-3 (1.90%)	1.37E+13 (0.35%)	0.87 (0.77%)

Figure 11: EIS characterization and equivalent circuit parameters for 4 cm long carbon rod electrodes spaced 1 cm apart before and after one experiment of 5 days of continuous electrical stimulation of 5V, 2 ms pulses delivered at 1 Hz from 4 cm carbon rods spaced 1 cm apart. The perturbation voltae was 10 mV. The effect of one experiment's worth of aging on the carbon rod electrodes is that the electrode's CPE has dramatically increased, but its polarization resistance remains largely unchanged. Moreover, the electrode behaves less-ideally like a capacitor, as evidenced in the drop in η after ageing.

Figure 11 shows Nyquist and Bode plots in addition to the calculated equivalent circuit parameters for carbon rods before and after a single experiment involving the delivery of 5 V, 2 ms pulses at a rate of 1 Hz for a total of 5 days. Most notable is the decrease in the electrode's CPE value, representing a lower impedance to charge injection. In addition, the electrode's Rp value decreased by a factor of two and its η value decreased as well. The importance of the decrease in Rp value is probably not very much compared to the decrease in CPE, since the Rp value, in absolute terms, is still very high, and approaches the measurable limit of this setup.

3.1.5. Input Voltage

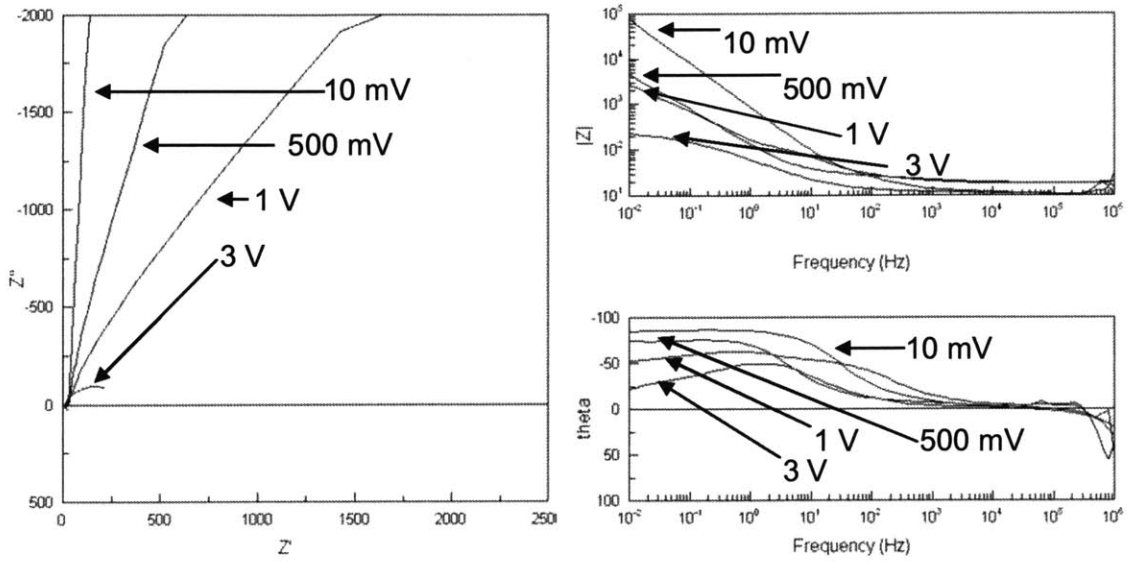

Input voltage	Rs, Ω (% error)	CPE/cm² (% error)	R_p Ω/cm² (% error)	η (% error)
10 mV	18.89 (0.93%)	9.07E-4 (0.90%)	5.59E+14 (0.02%)	0.91 (0.28%)
500 mV	21.24 (1.63%)	1.82E-3 (2.13%)	1.23E+13 (0.54%)	0.78 (1.02%)
1 V	10.51 (2.77%)	1.74E-3 (2.42%)	4.33E+12 (1.78%)	0.56 (1.14%)
3 V	11.08 (1.53%)	5.79E-3 (3.59%)	327.6 (5.67%)	0.60 (1.95%)

Figure 12: EIS characterization and equivalent circuit parameters for carbon rod electrodes measured with a range of perturbation voltages. With increased perturbation, the polarization resistance, η and CPE all decrease.

Figure 12 shows Nyquist and Bode plots in addition to the calculated equivalent circuit parameters for carbon rods characterized at increasing perturbation voltages. Although carbon electrodes are characterized by their high resistance to corrosion (evident by their high Rp values), this property is dependent on the voltage applied to them. When carbon rods are characterized with higher and higher perturbation voltages, their resistance to corrosion falls dramatically. Moreover, their resemblance to an ideal capacitor decreases, as evidenced by their decreasing η value, and the observed CPE value increases, indicating that the charge injection capacity increases.

3.1.6. Carbon rods in PBS versus DMEM +10% serum

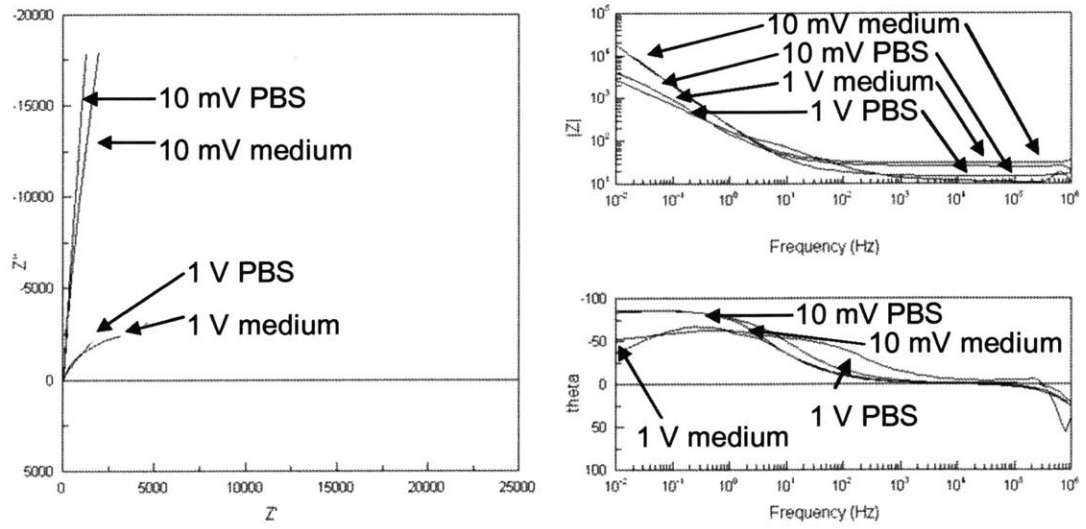

Input voltage	Rs, Ω (% error)	CPE/cm^2 (% error)	R_p Ω/cm^2 (% error)	η (% error)
10 mV	32.34 (0.81%)	7.52E-4 (1.00%)	1.21E+14 (0.05%)	0.92 (0.05%)
1 V	26.46 (0.70%)	1.52E-3 (1.03%)	6.75E+3 (5.13%)	0.78 (0.52%)

Figure 13: EIS characterization and equivalent circuit for carbon rod electrodes in a PBS versus DMEM+10% serum culture medium for electrodes 4 cm long and 1 cm apart. Table of calculated equivalent circuit parameters is for the DMEM solution.

Figure 13 shows Nyquist and Bode plots in addition to the calculated equivalent circuit parameters for carbon rods characterized in both a 1x PBS solution and a DMEM solution containing 10% serum, and at perturbation voltages of 10 mV and 1 V. It is worth noting that the calculated Rp values for both solutions calculated at a 10 mV perturbation voltage are both very high, but that at 1 V, the difference between the solutions is much more pronounced. The difference in the calculated η terms for the two solutions is also much greater for the higher perturbation voltage. Because the difference in measured solution resistance (32.34 Ω (medium) – 18.89 Ω (PBS)= 13.45 Ω) is greater than that for the theoretical values (55.8 Ω (medium) – 49.2 Ω (PBS) = 6.6 Ω) and because the Rp and η values change much more dramatically for culture medium than the PBS solution with higher perturbation voltages, it is likely that systems comprised of PBS and medium differ not only by their conductivity but also because of the interactions of the proteins contained within the serum.

3.1.7. Current Injection

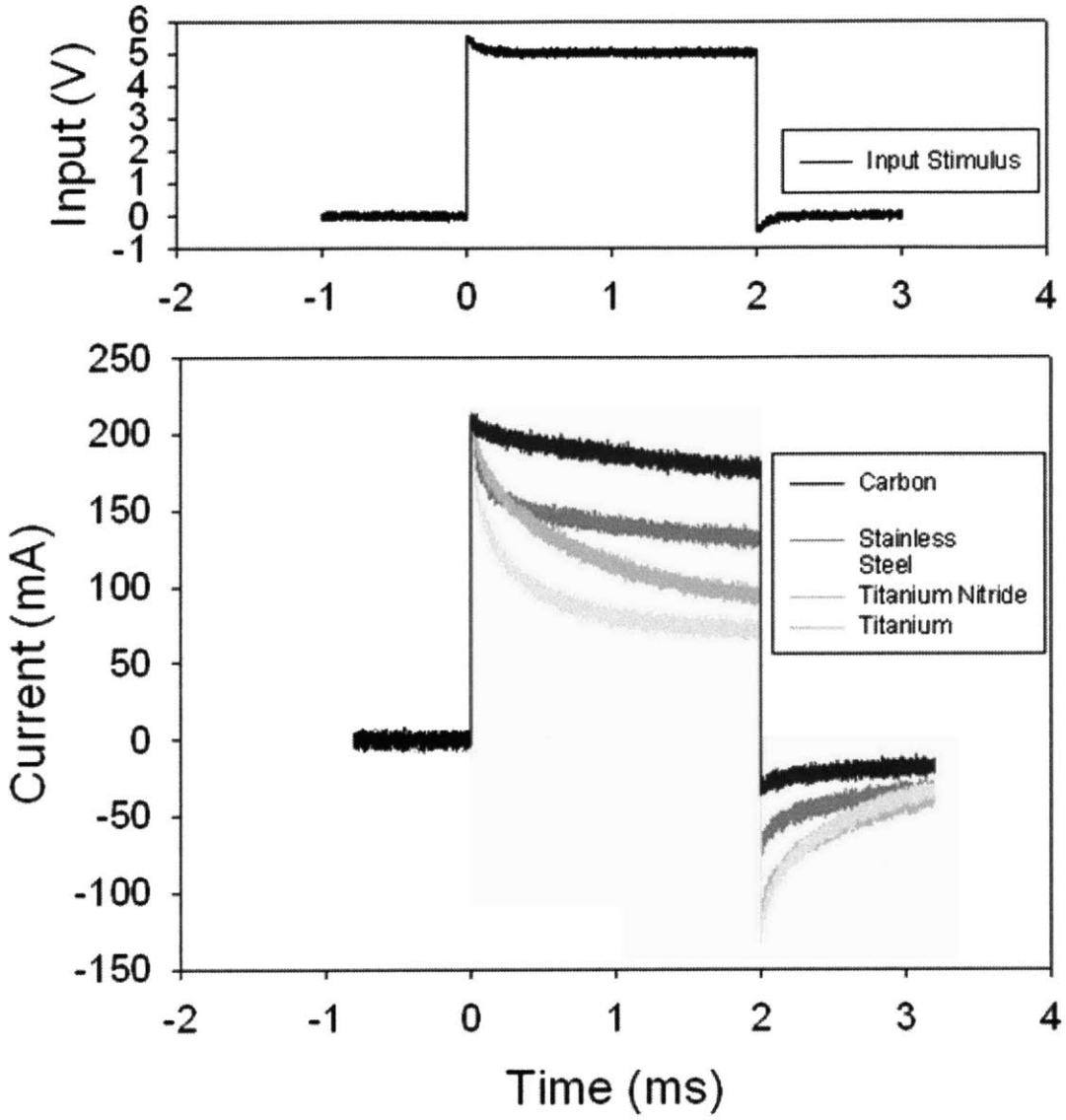

Material	Injected Charge (C)	Unrecovered Injected Charge (C)	% Injected Charge Unrecovered
Carbon	3.64e-4	5.64e-5	15.5%
Stainless Steel	2.81e-4	5.92e-5	21.1%
Titanium Nitride	2.35e-4	4.00e-5	17.0%
Titanium	1.80e-4	4.52e-5	25.1%

Figure 14: Current measured in bioreactor over 5 V, 2 ms square wave pulse, along with calculated injected charge and unrecovered injected charge (see **Section 2.3.2** for methods of calculation). The total net amount of injected charge in coulombs is equal to area beneath each curve at that time point.

Figure 14 shows the current measured in a bioreactor comprised of pairs of 4 cm long, parallel electrodes placed 1 cm apart, and composed of different electrode materials, during a sample stimulus. The applied stimulus in this case was a 2 ms long monophasic square pulse of 5 V amplitude. What is most notable in the comparison of the current injection characteristics of the four electrodes is that carbon electrodes, while injecting the most charge per pulse, also lose the least amount of charge per pulse to irreversible reactions. The fact that carbon loses any charge at all to irreversible reactions indicates that its Rp value at 5 V perturbation is low enough to make a measurable difference.

In the absence of an expensive EIS setup, current injection measurements inform the bioreactor designer with very useful information regarding not only the amount of charge injected, but the speed at which it is injected, the speed of recovery from a stimulus waveform, and the amount of charge diverted to irreversible reactions. The carbon electrodes, although recovering the most charge from the input stimulus, do so at the slowest rate (~60 mS versus ~30 ms for the other electrode materials). This rate might have implications for a bioreactor design employing higher stimulus frequencies than the 1 Hz rate considered in this study.

3.2. BIOREACTOR AND STIMULATOR DESIGN

3.2.1. Bioreactor Design

A bioreactor in general must be designed to provide both environmental control and biophysical signaling. In this study, the device provides 2 ms monophasic square pulses to the cells within it, and the bandwidth for this type of pulse is under 1 KHz, as shown in **Figure 15**, which allows us to make the electroquasistatic approximation for estimating the electric field lines for the stimulus (see Section 1.3.1) and also a sense of the bandwidth of interest in the various electrode's Bode plots. The bioreactor design must allow for this electrical stimulus to have a high charge injection, be consistent from experiment to experiment, and to come from electrodes which neither corrode nor create harmful reaction products in the culture medium. To accomplish this task we employ carbon rod electrodes which are replaced after each experiment.

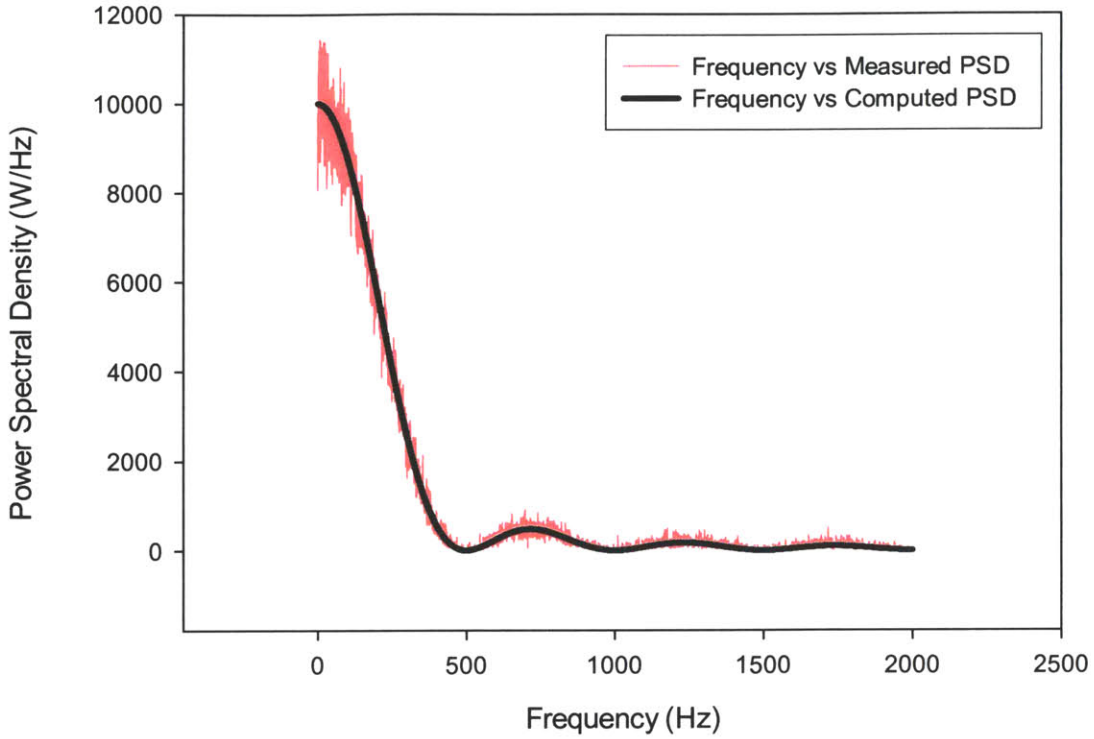

Figure 15: Power spectral densities calculated for (black) an ideal pulse of amplitude 5 V, 2 ms duration, delivered at a frequency of 1 Hz, and (pink) a measured pulse delivered from the cardiac stimulator employed in this study with the same parameters. More than 90% of stimulus power is in the bandwidth < 1 kHz for the measured pulse, which agrees with the theoretical calculation.

To assess cell alignment after stimulation, it is desirable to maintain a constant alignment of scaffolds with respect to the direction of the electric field gradient, while at the same time not restricting the contractions of the tissue construct nor the ability to observe the constructs with a microscope. We accomplish this task using stainless-steel pins, held in place by a thin layer of PDMS at the bottom of a Petri dish, as shown in **Figure 6**.

One of the merits of this bioreactor design is that it is composed of inexpensive parts which are easy to handle, and autoclavable. Some drawbacks include the extra handling involved in positioning the scaffolds between the electrodes and the possibility of the interference of the stainless steel pins with the applied electric field stimulus and with contractions of the tissue engineered constructs. In order to avoid such problems, it is necessary to exercise extra care during handling.

3.2.2. Stimulator Design

A good stimulator should be able to accommodate a wide range of bioreactor configurations while delivering electrical stimuli in a faithful manner. Moreover, an ability to program a wide range of pulse shapes will likely be useful. In order to capitalize on the programming capabilities provided for LabView® analog output cards, an experimental setup including a stimulator based upon a computer-controlled LabView® output card was employed, along with an amplifier circuit, as shown in **Figure 5**, because the maximum current rating of the employed card is only 20 mA. The design of the amplifier was based upon an operational amplifier wired in unity-gain mode, as shown in **Figure 16**, and the specific chip used was the OPA-551 from Burr-Brown, chosen for its high current rating (200 mA), high voltage range (-12 V through +12 V) and stability in unity-gain configuration.

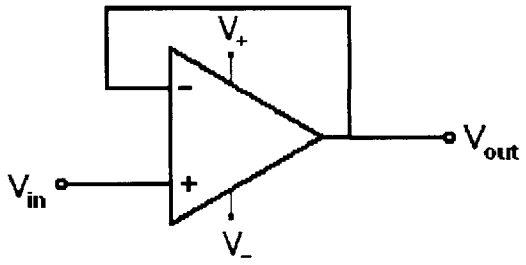

Figure 16: Operational Amplifier in unity gain mode. Device must be unity-gain-stable to be used in this configuration.

When a stimulator's current rating is below that which the attached load requires, the stimulus waveform is not faithfully applied to the load, as shown in **Figure 17**, and this situation is highly undesirable.

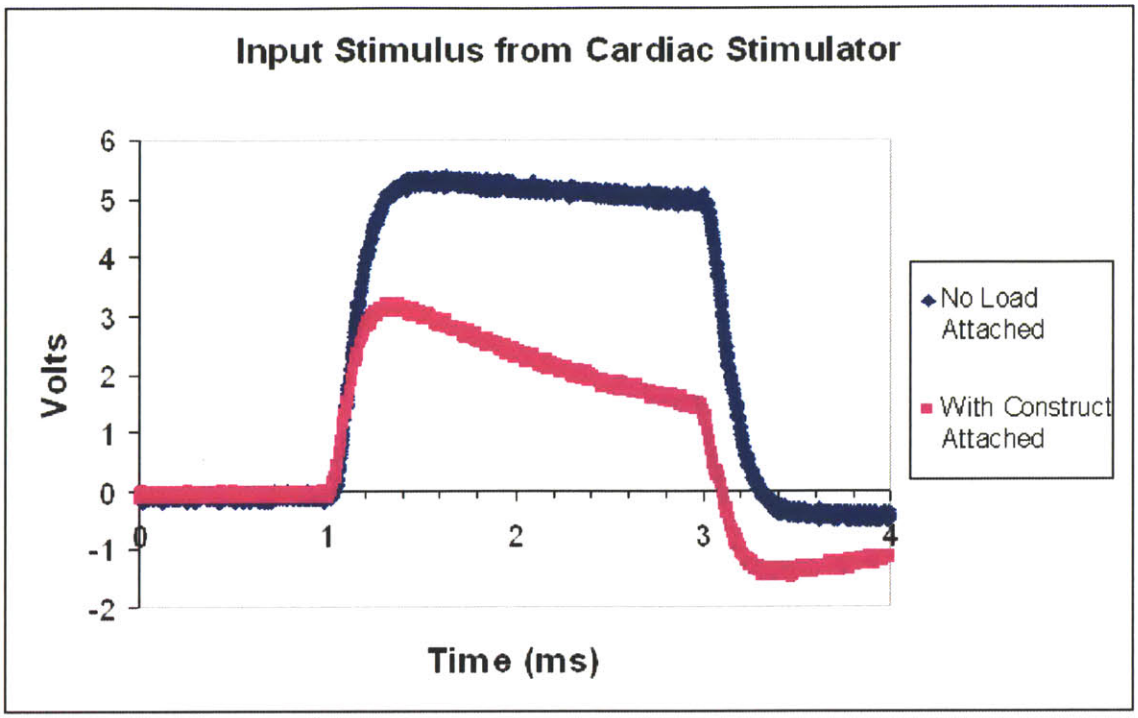

Figure 17: Stimulus waveform from commercial stimulator with low current rating. When a bioreactor is attached (pink), the stimulus waveform (blue) is no longer faithfully applied.

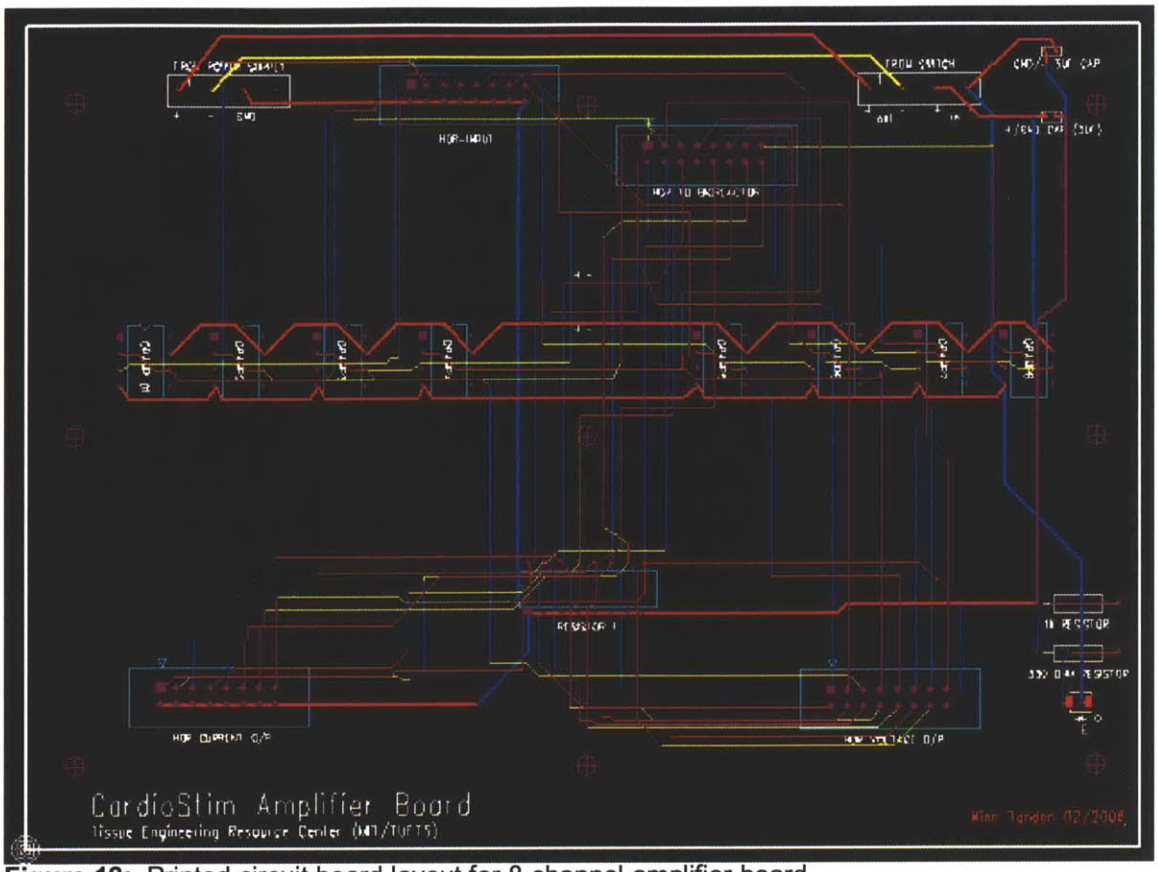

Figure 18: Printed circuit board layout for 8-channel amplifier board.

Figure 18 shows the printed circuit board layout for the amplifier circuit designed for this stimulator. The circuit board interfaces with any input stimulus generator, including the LabView card used in this study, and allows for eight separate channels of amplification. Additionally, outputs such as the applied voltage and current through the bioreactor can be measured online.

3.3. BIOLOGICAL RESULTS

3.3.1. Functional Results

In order to exhibit the normal contractile behavior of a synctium in vivo, it is necessary for cardiomyocytes to express functional gap junctions, cytoskeletal organization, and excitation–contraction coupling. It has been hypothesized that electrical stimulation enhances the development of ultrastructural and contractile properties of individual cells as well as increasing the numbers of electrically coupled cells [5]. In this study, the levels of electrical stimulation were modulated via two mechanisms: electrode spacing and stimulation amplitude.

3.3.1.1. Modulating Electric Field Stimulus via Electrode Spacing

The experimental setup for this test is as shown in **Figure 19**. Scaffolds were stimulated with varying electric field strengths by being placed at increasing distances from the electrodes.

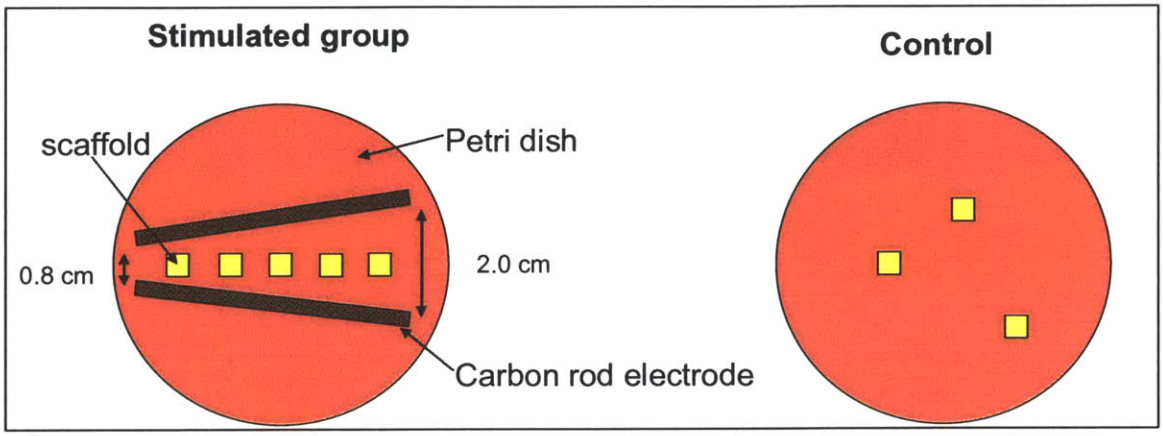

Figure 19: Experimental setup for study involving the modulation of electric field strength via electrode spacing. Stimulated group was submitted to monophasic, square pulses of 2 ms in duration and 1 Hz frequency. Electric field stimulus was modulated by the spacing of the electrodes.

Figure 20 shows the average measured excitation thresholds and maximum capture rates for the scaffolds. The collected experimental data is consistent with the hypothesis that the applied electric field stimulus can be optimized, since there appears to be a local minimum for excitation threshold corresponding to increasing electric field stimuli, as well as a local maximum for maximum capture rate. Moreover, there also appears to be a maximum safely applied stimulus.

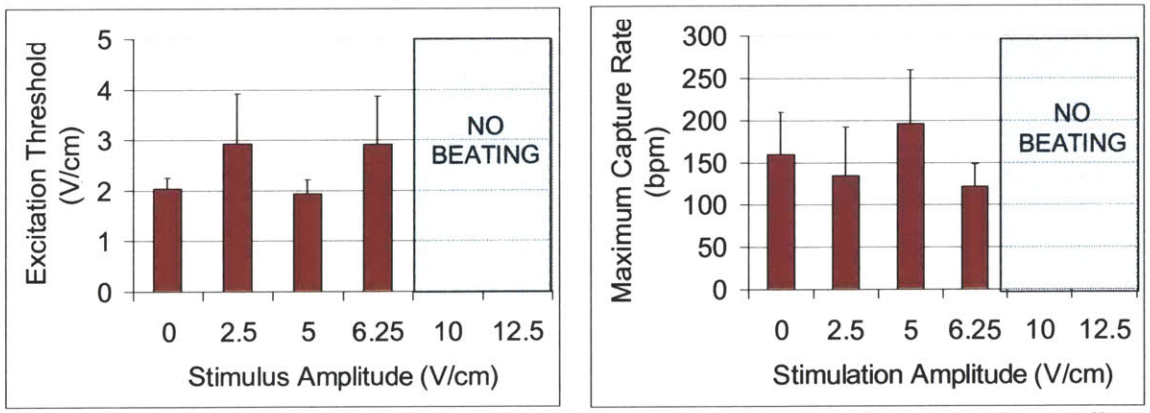

Figure 20: The measured excitation thresholds and maximum capture rates for scaffolds stimulated at various levels in culture. Of the stimulated constructs, there is a decrease and subsequent increase in excitation threshold, corresponding to an increase and subsequent decrease in maximum capture rate. At stimulation levels >= 10 V/cm, there was no observed contraction, suggesting that there is an optimal level of stimulation below this level.

3.3.1.2. Modulating Electric Field Stimulus via Stimulation Amplitude

In the second experimental setup, shown in **Figure 21,** electric field intensity was modulated via the amplitude of the stimulus waveform applied to the electrodes.

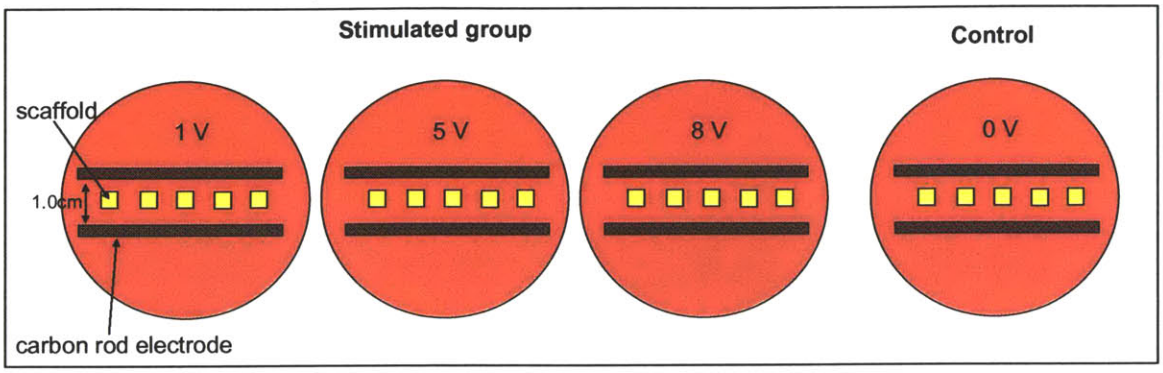

Figure 21: Experimental setup for study involving the modulation of electric field strength via stimulation amplitude. Stimulated group was submitted to monophasic, square pulses of 5V in amplitude, 2 ms in duration and 1 Hz frequency. Electrode spacing was kept constant at 1.0 cm and the electric field stimulus was modulated by the increasing amplitude of the stimulus waveform.

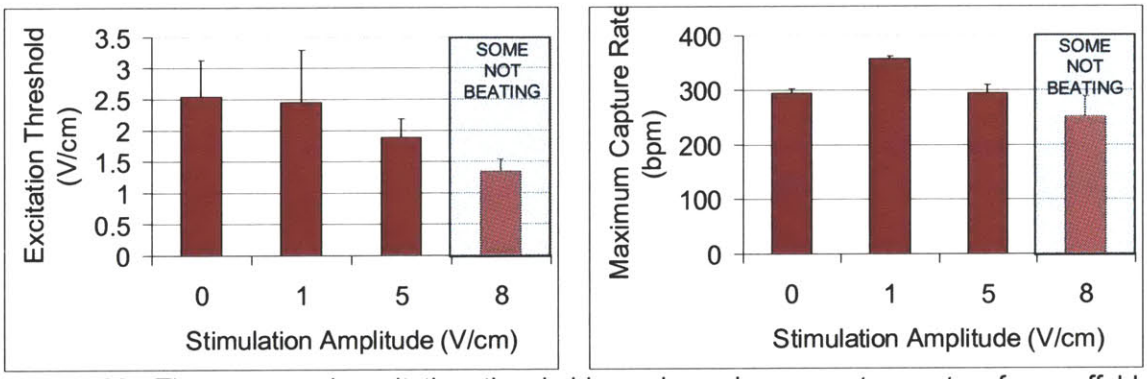

Figure 22: The measured excitation thresholds and maximum capture rates for scaffolds stimulated at various levels in culture. There is a decrease in excitation threshold accompanying increasing levels of electrical stimulation, although at stimulation levels >= 8 V/cm, there was some observed lack of contraction, suggesting that there is an optimal level of stimulation below this level. Maximum capture rates also increased at stimulation levels <=5V/cm, but decreased for stimulation = 8V/cm, at which point not all scaffolds were induced to contract, again suggesting that optimal stimulation levels are < 8 V./cm.

Figure 22 shows the average measured excitation thresholds and maximum capture rates for the scaffolds cultured under this condition. Again, the collected experimental data is consistent with the hypothesis that the applied electric field stimulus can be optimized, since there appears to be a local minimum for excitation threshold corresponding to increasing electric field stimuli, as well as a local maximum for maximum capture rate. Moreover, there again appears to be a maximum safely applied stimulus.

When comparing the data from the two sets of experiments, it is interesting to note that the location of the "optimal" stimulation amplitude has shifted from the first experimental condition to the second. That is, for the first experiments, the "sweet spot" of electrical stimulus (that is, the stimulus providing the lowest excitation threshold and simultaneously the highest maximum capture rate) seems to be hover around 5 V/cm. For the second set of experiments, however, the location of the "sweet spot" seems to hover around 1 V/cm. It is worth noting that the highest maximum capture rates (for 1 V/cm in the stimulation amplitude-group) were recorded for the scaffolds exposed to the least amount of electrical stimulation and reaction products

This shift is most likely connected to the key difference between these two experiments, which is the level of exposure of the constructs to the reaction products resulting from the irreversible faradaic reactions occurring during stimuli. To elaborate, in the first experiment, constructs stimulated at all levels were exposed to the same level of reaction products, and those under the control condition were not exposed to any at all. For the second set of conditions, however, scaffolds stimulated at increasing levels of electric field stimuli were exposed to a corresponding increase in faradaic reaction products. Since the level of faradaic reactions is known to be exponentially related to applied voltage [61] it can be assumed that all the scaffolds in the first experimental condition were exposed to levels of reaction products higher than that of the 5 V/cm condition in the second experimental condition.

The combined effects of electrical stimulation and faradaic reaction products cannot be decoupled in this study, but in the future, a perfusion system would allow decoupling of these effects.

3.3.2. Morphological Results

A fundamental tenet of anatomy and physiology is that any functional attributes of a given biological system must be rooted in some way to structural elements. For this reason, we look to changes in cell and tissue morphology for insight into the observed functional changes described in this study. One functional observation is that the constructs stimulated at a level of 1 V/cm exhibited both the lowest excitation threshold, as well as the highest maximum capture rates.

Perhaps a link between this observation and the tissue morphology is the progressive lack of survival of the non myocytes (mainly fibroblasts) in culture, as shown in **Figure 23**, which shows confocal images of constructs stimulated at progressively increasing levels, and stained for cardiac troponin-I (green, for myocytes), vimentin (red, for non-myocytes) and cell nuclei (blue).

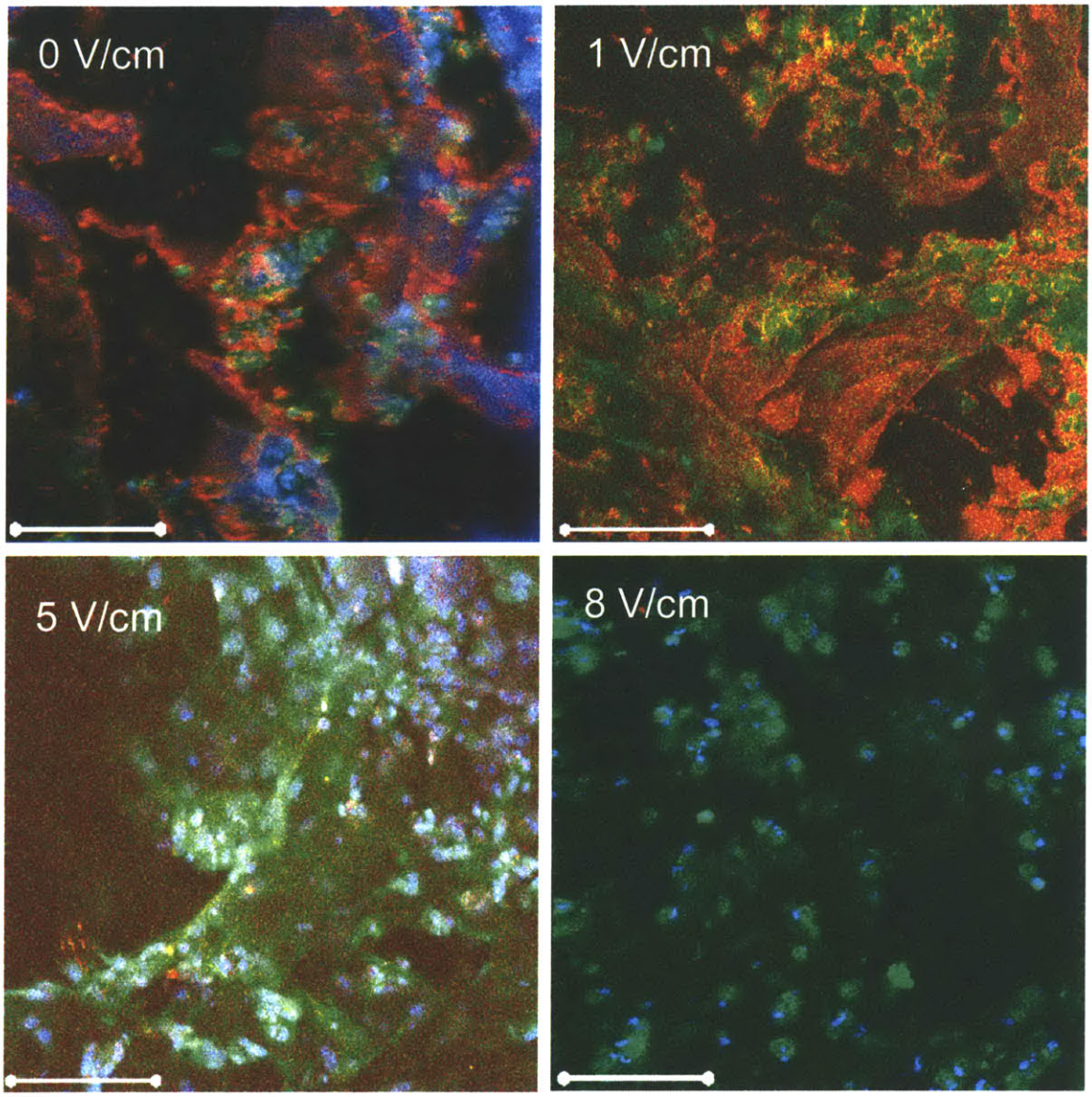

Figure 23: Confocal images of engineered tissue constructs stained for Troponin-I (green, cardiomyocytes), Vimentin (red, non-mocytes) and cell nuclei (bliue). White bar corresponds to 100 μm. With increasing levels of stimulation, the density of non-myocytes appears to decrease.

Although the protocol for the isolation of ventricular myocytes employed in this study utilizes a preplating step in order to purify the sample of myocytes from the presence of fibroblasts, in reality, the presence of the fibroblasts is never truly eliminated. **Figure 23** shows images obtained via confocal microscopy of tissue engineered constructs stimulated with increasing levels of stimulation. The constructs were stained with cardiac troponin-I, a marker for cardiomyocytes, and vimentin, expressed in mesenchymal cells such as fibroblasts, smooth muscle cells, and endothelium [62], and thus a marker for all non-myocytes in the constructs (which are mainly fibroblasts in this preparation). It is interesting to note the appearingly inverse relationship between the survival rate of the non-myocytes (mainly fibroblasts) with progressively increasing levels of electrical stimulation, implying that the presence of fibroblasts leads to healthier constructs. This observation, if true, would affirm the recent independent observation that co-culture conditions, even in the absence of electrical stimulation, lead to improved engineered cardiac tissue constructs [63]. In addition, it appears that although cardiac cells (stained in green) appear elongated at stimulation levels of 1 V/cm and 5 V/cm, they do not appear very different in terms of their elongation, and indicate that induced elongation may be an "all or nothing" effect, akin to that of the action potential itself. These results suggest that perhaps higher levels of stimulation, in combination with higher levels of reaction products, are toxic to the cells. A perfusion-based system, washing away harmful reaction products, would help decouple these two effects.

Another benefit to a perfusion-based system would be to allow the engineering of thicker cardiac constructs. As shown in **Figure 24**, cells residing at the penetration depth of oxygen (100 μm below the surface) appear rounded in shape, and probably contribute very little to the contractions of the construct. A perfusion-based bioreactor system would allow for the increase of the thickness of healthy engineered cardiac tissue.

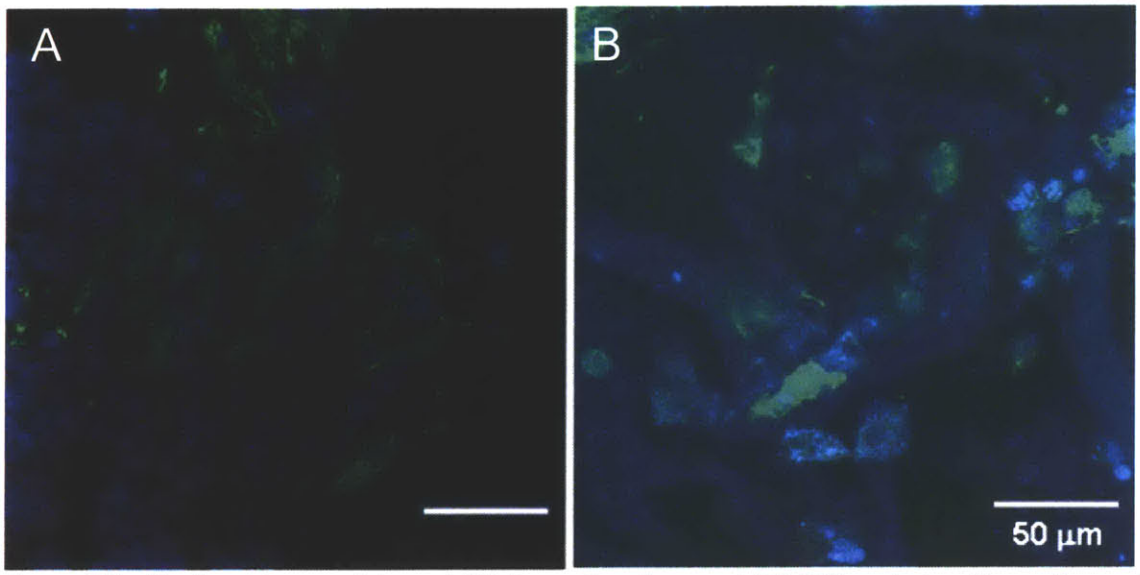

Figure 24: Confocal images taken at (A) the cell surface and (B) 100μm below the surface, of constructs stained for cardiac Troponin-I (green) and cell nuclei (blue). Cells 100 μm below the surface appear round and unhealthy. This distance corresponds to the penetration depth of oxygen, indicating that a perfusion based system may allow the engineering of thicker constructs.

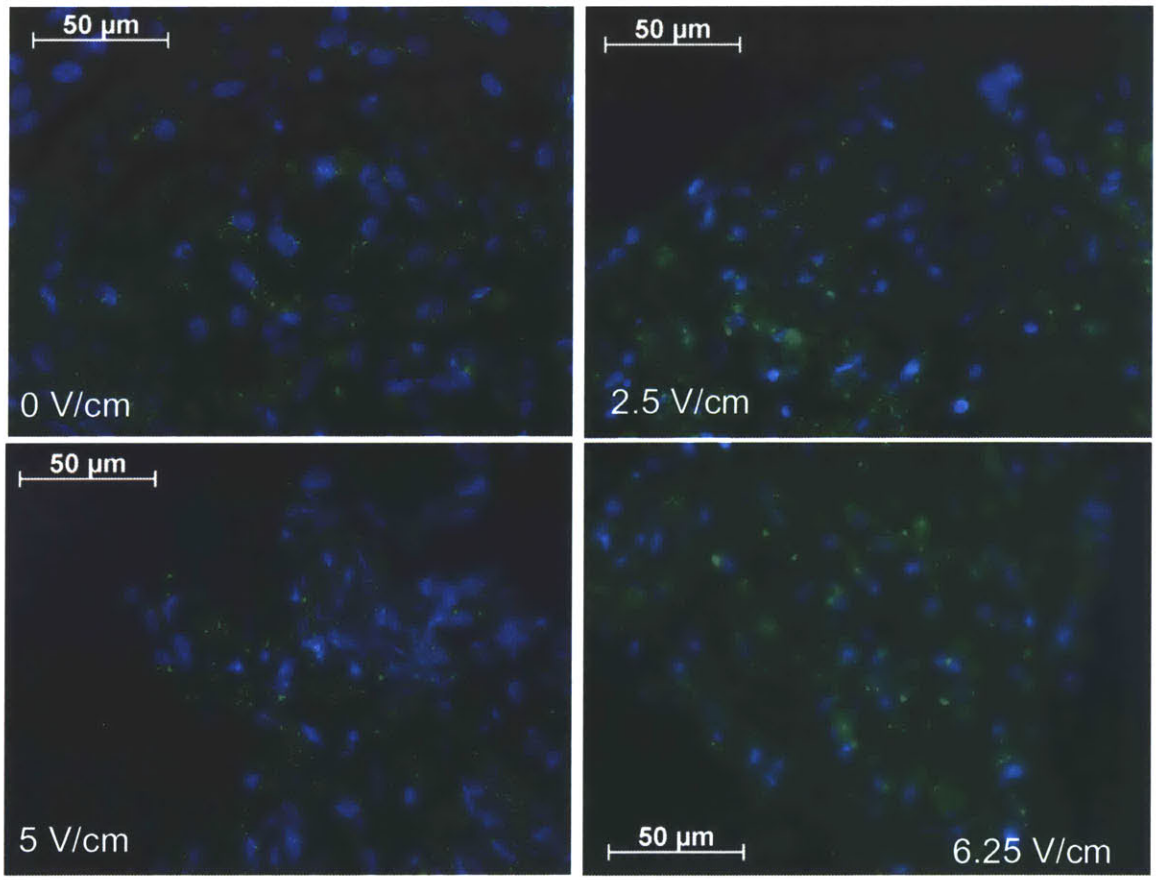

Figure 25: Constructs stained for connexin-43 (green) and cell nuclei (blue). Connexin-43 resides less in the cell's cytosol at the stimulation amplitude of 5 V/cm than for stimulation amplitudes of either 2.5 V/cm or 6.25 V/cm.

Another cellular-based indication of the link between the contractile behavior of the engineered tissue constructs is the link between the formation of gap junctions and the levels of stimulation during culture, as shown in **Figure 25**. Again, there appears to be an optimum voltage gradient, as indicated by the more punctuated distribution of Cx-43 in constructs stimulated at 5 V/cm which was associated with higher maximum capture rate in these constructs and lower excitation thresholds, as compared to constructs stimulated at other levels. Further studies are being undertaken to interrogate these effects in more detail.

It is interesting to note that although the cultured rat ventricular myocytes exhibited elongation with electrical stimulation, an important characteristic of native heart tissue, they did not exhibit any preferred direction of alignment, which is another important characteristic of native heart tissue. In contrast, however, C2C12 cells cultured under identical conditions to the rat ventricular myocytes, exhibited not only elongation in response to the electrical stimuli, but also a remarkable amount of alignment, as shown in **Figure 26**. This observation may be linked to the more mature nature of the rat ventricular myocytes to the C2C12 myoblast cell line, but in any event, elongation in addition to alignment is an important characteristic of native heart tissue, and so should be investigated further.

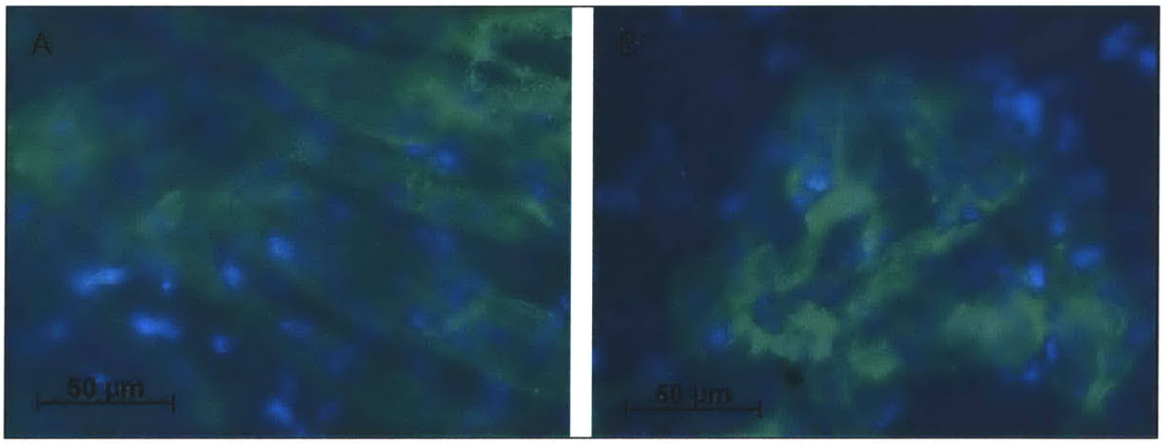

Figure 26: Elongation of C2C12 cells stimulated on collagen scaffolds. C2C12 cells stained for cardiac Troponin-I (green) and DAPI for cell nuclei (blue). A. Scaffolds subjected to stimulation of 5V, 2 ms pulses delivered at 1 Hz for 5 days of culture show remarkably more alignment in addition to elongation than B. those not subjected to any electrical stimulation.

4. SUMMARY AND FUTURE WORK

4.1. SUMMARY

After the completion of this study, a number of conclusions may be drawn. Porous carbon has been identified as the electrode with the highest amount of current injection with the smallest percentage of irreversible reaction product, although its porosity increases the amount of time necessary to recover from an applied stimulus. Furthermore, despite the high resistance of the porous carbon to reactions, the level of reaction products has been identified as an additional variable to be considered in all other future experiments.

Despite the detrimental effect of reaction products, further optimization of electrical stimulation has been achieved, and a maximum safe applied voltage of 8 V/cm for the 2 ms monophasic pulses employed in this study at 1 Hz has been identified, although the upper limit for the survival of fibroblasts, which may improve contractile function, may in fact be much lower. Whatever the value, it may potentially be increased with the utilization of a perfusion mechanism to wash away reaction products from cultured cells.

In terms of stimulator design, a number of design recommendations may be made after the completion of this study, including the use of stimulation apparatus with a current rating matching that of the bioreactor requirements, and the inclusion of the capability to monitor the applied stimulus and the current profiles within the bioreactor during all experiments.

4.2. FUTURE WORK

4.2.1. Cell Culture

Although Matrigel has been employed in this study for rapid cell inoculation into scaffolds, and serum has been employed to aid in cell culture in this study, their components are not fully characterized and so their use adds a measure of uncertainty to experiments. In addition to decreasing the uncertainty of culture conditions, serum- and Matrigel-free culture conditions are expected to reduce immunogenicity of engineered cardiac tissue constructs.

It has recently been reported that Matrigel may be replaced with insulin and triiodothyronine, and that supplementation of culture medium with certain growth

factors may allow for serum-free conditions, in the presence of co-culture conditions of myocytes with endothelial cells [63]. This study, however, did not employ any electrical stimulation for culture conditions. An important area of future work is therefore to attempt co-culture of myocytes with other cell types endogenous to the heart, under Matrigel- and serum- free conditions, with electrical stimulation.

4.2.2. Further experiments

Areas of future work for this study include incorporating further analysis of the effects of modulated electric field stimulation on engineered cardiac tissue, by varying frequency, field gradient, initiation, duration and wave shape of the stimulus, for example. In addition, quantifying the effect of electrical field stimulation on other cell types present in the native myocardium (endothelial cells and fibroblasts) is of the utmost importance for developing co-culture strategies. This work is already underway, and preliminary results indicate that there exists not only an optimum level of stimulation, but also an optimal combination of DC and AC stimulation for elongation and alignment of cells in engineered tissue. Given the high number of parameters at work, in order to accomplish these tasks, high throughput approaches are needed to determine optimal stimulation parameters, and developing these methods is another important area of future work.

In addition, in order to tease apart biological pathways, it may be useful to perform pharmacological analysis of the tissue engineered constructs, by culturing them in the presence of various channel blockers. In the future, an investigation of gene expression of certain cardiac proteins such as: Myosin light chain, connexin 43, other target genes, atrial natiuretic factor may be performed. Lastly, in vivo testing of the biological function and remodeling of the cardiac grafts after implantation in injured myocardium is another important area of future work.

4.2.3. Bioreactor Design

In addition to performing further analysis, the bioreactor setup may also be improved. In order to reduce the number of variables between this study and other studies investigating electrical stimulation, in particular that conducted by Radisic et al., scaffolds are maintained under static culture in this bioreactor

setup. Since the 3-D cell constructs developed in this study lack the vascular network that exists in normal vascularized tissues, gas and nutrient supply to the scaffold-seeded cells depend merely on mass diffusion, and so large diffusional gradients are expected to be formed between the cell constructs and their surroundings, and oxygen transport is expected to be a main limiting factor for nutrient exchange. Nonetheless, a perfusion setup was not employed at this stage in order to simplify the bioreactor setup and allow freedom for manipulating other elements of the bioreactor, most notably distance between the electrodes, and ensuring that the scaffolds were maintained in a consistent orientation with respect to the electrodes. In addition, trends in response to the amplitude of stimulation were expected to be somewhat independent of cell number, and so the implementation of perfusion capabilities was postponed. Incorporating perfusion capabilities into the bioreactor setup, however, is of the utmost importance because is necessary not only to produce thicker tissue constructs, however, but also in order to eliminate the possible detrimental effects of electrode/electrolyte reaction products from the culture medium.

In terms of electrode choice, another area of future work might be to test certain other materials, including stainless steel alloys h P558 and of AISI 316L, which may have a higher degree of biocompatibility than the 303 alloy tested in this study.

4.2.4. Development of better readouts

Another important area of future work involves developing better analytical tools to allow for more precise readouts. In particular, the measure of threshold voltage may be made more precise if only a section of the tissue is stimulated, rather than the entire scaffold, as it was in this study. When the entire scaffold is stimulated at once, the effects of the cell-to-cell coupling and the density of ion channels are not easily separated. Indeed, in a previous study utilizing this same method for measuring excitation threshold, although there was a marked difference in maximum capture rate from electrical stimulation, there was no observed statistical difference in the threshold voltage they measured for stimulated and unstimulated constructs [5]. In addition, in order to better quantify the constructs' maximum capture rate, the development of a system incorporating a closed-loop feedback system or electrocardiographic measurements may be of use.

5. REFERENCES

1. *Heart Disease and Stroke Statistics: 2005 Update*. 2005, American Heart Association.
2. Zammaretti, P. and M. Jaconi, *Cardiac tissue engineering: regeneration of the wounded heart.* Current Opinion in Biotechnology, 2004. **15**(5): p. 430-434.
3. Radisic, M., et al., *Biomimetic Approach to Cardiac Tissue Engineering: Oxygen Carriers and Channeled Scaffolds.* Tissue Engineering. **12**(8).
4. Leor, J. and S. Cohen, *Myocardial Tissue Engineering: Creating a Muscle Patch for a Wounded Heart.* Ann NY Acad Sci, 2004. **1015**(1): p. 312-319.
5. Radisic, M., et al., *From the Cover: Functional assembly of engineered myocardium by electrical stimulation of cardiac myocytes cultured on scaffolds.* PNAS, 2004. **101**(52): p. 18129-18134.
6. Radisic M, P.H., Gerecht-Nir S, Cannizzaro C, Langer R., Vunjak-Novakovic G. , *Biomimetic approach to cardiac tissue engineering.* . Philosophical Transactions of the Royal Society of London (in press).
7. Eghbali, M., et al., *Cardiac Fibroblasts are Predisposed to Convert into Myocyte Phenotype: Specific Effect of Transforming Growth Factor {beta}.* PNAS, 1991. **88**(3): p. 795-799.
8. Brutsaert, D.L., *Cardiac Endothelial-Myocardial Signaling: Its Role in Cardiac Growth, Contractile Performance, and Rhythmicity.* Physiol. Rev., 2003. **83**(1): p. 59-115.
9. Severs, N., J. , *The cardiac muscle cell.* BioEssays, 2000. **22**(2): p. 188-199.
10. Manjunath CK, G.G., Page E, *Human cardiac gap junctions: isolation, ultrastructure, and protein composition.* J Mol Cell Cardiol., 1987. **19**(2): p. 131-4.
11. Hotary, K., Robinson KR., *Endogenous electrical currents and voltage gradients in Xenopus embryos and the consequences of their disruption.* Developmental biology, 1994. **166**(2): p. 789-800.
12. Nuccitelli, R., *Endogenous Ionic Currents and DC Electric Fields in Multicellular Animal Tissues.* Bioelectromagnetics. , 1992. **Suppl 1**: p. 147-57.
13. Levin, M., *Motor protein control of ion flux is an early step in embryonic left–right asymmetry.* BioEssays 2003. **25:**: p. 1002-1010.
14. Ypey DL, C.D., DeHaan RL., *Development of electrical coupling and action potential synchrony between paired aggregates of embryonic heart cells.* The Journal of membrane biology., 1979. **51**(1): p. 75-96.
15. Rutenberg, J., SHING-MING CHENG, MICHAEL LEVIN, *Early Embryonic Expression of Ion Channels and Pumps in Chick and Xenopus Development.* DEVELOPMENTAL DYNAMICS, 2002(225): p. 469–484.
16. Goldstein, A.M., Baruch S. Ticho Mark C. Fishman, *Patterning the heart's left-right axis: From zebrafish to man.* Developmental Genetics, 1998. **22**(3): p. 278-287.
17. Veenstra, R.D. and R.L. DeHaan, *Electrotonic interactions between aggregates of chick embryo cardiac pacemaker cells.* Am J Physiol Heart Circ Physiol, 1986. **250**(3): p. H453-463.
18. Costanzo, L., *Physiology*. Vol. 2nd, rev ed. 2002, Philadelphia: Saunders.
19. Peters, N.S. and A.L. Wit, *Myocardial Architecture and Ventricular Arrhythmogenesis.* Circulation, 1998. **97**(17): p. 1746-1754.
20. Nian, M., et al., *Inflammatory Cytokines and Postmyocardial Infarction Remodeling.* Circ Res, 2004. **94**(12): p. 1543-1553.

21. Smith, J.H., et al., *Altered patterns of gap junction distribution in ischemic heart disease. An immunohistochemical study of human myocardium using laser scanning confocal microscopy.* Am J Pathol, 1991. **139**(4): p. 801-821.
22. Tomaselli, G.F. and D.P. Zipes, *What Causes Sudden Death in Heart Failure?* Circ Res, 2004. **95**(8): p. 754-763.
23. Ursell, P.C., et al., *Structural and electrophysiological changes in the epicardial border zone of canine myocardial infarcts during infarct healing.* Circ Res, 1985. **56**(3): p. 436-451.
24. Kocher, A.A., et al., *Neovascularization of ischemic myocardium by human bone-marrow-derived angioblasts prevents cardiomyocyte apoptosis, reduces remodeling and improves cardiac function.* Nature Medicine, 2001. **7**(4): p. 430.
25. Shimizu, T., et al., *Fabrication of Pulsatile Cardiac Tissue Grafts Using a Novel 3-Dimensional Cell Sheet Manipulation Technique and Temperature-Responsive Cell Culture Surfaces.* Circ Res, 2002. **90**(3): p. 40e-48.
26. Durand, D., and Bronzino, J.D. Editor, *Electric Stimulation of Excitable Tissue.* The Biomedical Engineering Handbook, 1995. **Chapter 17**: p. 229-251.
27. Merrill, D.R., Marom Bikson and John G.R. Jefferys, *Electrical stimulation of excitable tissue: design of efficacious and safe protocols.* Journal of Neuroscience Methods 2005 **141** (2): p. 171-98.
28. Vardalas, J. *Engineering and Pop Culture: Galvani and the Story of Frankenstein.* 2004 [cited June 20th 2005]; Available from: http://www.todaysengineer.org/2004/Apr/history.asp.
29. Finkelstein, E., et al., *Roles of microtubules, cell polarity and adhesion in electric-field-mediated motility of 3T3 fibroblasts.* J Cell Sci, 2004. **117**(8): p. 1533-1545.
30. Song, B., et al., *Nerve regeneration and wound healing are stimulated and directed by an endogenous electrical field in vivo.* J Cell Sci, 2004. **117**(20): p. 4681-4690.
31. Hart, R.A. and O.P. Gandhi, *Comparison of cardiac-induced endogenous fields and power frequency induced exogenous fields in an anatomical model of the human body.* Physics in Medicine and Biology, 1998. **43**(10): p. 3083-3099.
32. Tung, L.a.J.R.B., *Analysis of electric field stimulation of single cardiac muscle cells.* Biophysical Journal, 1992. **63**(2): p. 371-386.
33. Tovar, O. and L. Tung, *Electroporation and recovery of cardiac cell membrane with rectangular voltage pulses.* Am J Physiol Heart Circ Physiol, 1992. **263**(4): p. H1128-1136.
34. Bethune, D.S., et al., *Cobalt-catalysed growth of carbon nanotubes with single-atomic-layer walls.* Nature, 1993. **363**(6430): p. 605-607.
35. Ted Pella, I. [website] [cited; Available from: http://www.tedpella.com/carbon_html/carbon1.htm.
36. Ladd.Research.Industries, *Specification Sheet for Carbon Rods Ladd Catalog Number 30250.* 2006.
37. A. Norlin, J.P., and C. Leygra, *Electrochemical Behavior of Stimulation/Sensing Materials for Pacemaker Electrode Applications.* Journal of The Electrochemical Society, 2005. **152**(9): p. J110-J116.
38. Lee, G.-J., S.-I. Pyun, and C.-H. Kim, *Kinetics of double-layer charging/discharging of the activated carbon fiber cloth electrode: effects of pore length distribution and solution resistance.* Journal of Solid State Electrochemistry, 2004. **8**(2): p. 110-117.

39. McMaster-Carr. *Document 9051KAC More About Titanium, Nickel, and Tungsten Alloys.* 2007 [cited; Available from: http://www.mcmaster.com/.
40. A. Norlin, J.P., and C. Leygraf, *Investigation of Electrochemical Behavior of StimulationÕSensing Materials for Pacemaker Electrode Applications.* Journal of The Electrochemical Society, 2005. **152**(2): p. J7-J15
41. Eclat.Industries. *Eclat Coating Properties (Titanium Nitride).* [cited July 12th, 2006]; Available from: http://www.eclatcoating.com/products/coatingoverview.php.
42. Azom.com. *Stainless Steel - Grade 303.* AZo Journal of Materials Online 2006 [cited; Available from: http://www.azom.com/details.asp?ArticleID=964.
43. Montanaro L, C.M., Campoccia D, Prati C, Breschi L, Arciola CR, *No genotoxicity of a new nickel-free stainless steel.* International Journal of Artificial Organs., 2005 **28**(1): p. 58-65.
44. Macdonald, J., *Impedance spectroscopy.* Annals of Biomedical Engineering, 1992. **20**(3): p. 289-305.
45. Gamry.Instruments. *Electrochemical Impedance Spectroscopy Theory: A Primer.* 2005 [cited 2005 July 16th, 2006]; Available from: http://www.gamry.com/App_Notes/EIS_Primer/EIS_Primer.pdf.
46. Scully, J.R., Silverman, David C., Kendig, Martin W. Ed., *Electrochemical Impedance: Analysis and Interpretation.* 1993: ASTM International.
47. *Electrochemistry Encyclopedia.* 2006 [cited 2006 August 8th, 2006]; Available from: http://electrochem.cwru.edu/ed/encycl/index.html.
48. Johnson, D. *Equivalent Circuits - Circuit Elements.* Zview 2(R) help files 2002 [cited July 18th, 2006].
49. *Explaining a Constant Phase Element (CPE).* Research Solutions & Resources. August 8th, 2006 [cited; Available from: http://www.consultrsr.com/resources/eis/cpe2.htm.
50. Rashid, S.T., et al., *The use of animal models in developing the discipline of cardiovascular tissue engineering: a review.* Biomaterials, 2004. **25**(9): p. 1627.
51. Reinecke, H. and C.E. Murry, *Transmural Replacement of Myocardium after Skeletal Myoblast Grafting into the Heart: Too Much of a Good Thing?* Cardiovascular Pathology, 2000. **9**(6): p. 337.
52. Koh GY, K.M., Soonpaa MH, Field LJ., *Differentiation and long-term survival of C2C12 myoblast grafts in heart.* J Clin Invest, 1993. **92**(3): p. 1548-54.
53. Robinson SW, C.P., Levitsky HI, Olson JL, Hruban RH, Acker MA, Kessler PD., *Arterial delivery of genetically labelled skeletal myoblasts to the murine heart: long-term survival and phenotypic modification of implanted myoblasts.* Cell Transplant. , 1996. **5**(1): p. 77-91.
54. Blais, A., et al., *An initial blueprint for myogenic differentiation.* Genes Dev., 2005. **19**(5): p. 553-569.
55. U. Cheema, S.Y.Y.V.M.G.G.G.R.A.B., *3-D in vitro model of early skeletal muscle development.* Cell Motility and the Cytoskeleton, 2003. **54**(3): p. 226-236.
56. Vandenburgh, H.H., S. Swasdison, and P. Karlisch, *Computer-aided mechanogenesis of skeletal muscle organs from single cells in vitro.* FASEB J., 1991. **5**(13): p. 2860-2867.
57. Johnson, D. *Equivalent Circuits - Fitting Results.* Zview 2(R) help files 2002 [cited July 18th, 2006].
58. S.D. Bird, P.A.D., *The human adult cardiomyocyte phenotype.* Cardiovascular Research, 2003. **58**(2).

59. Gilchrist, K.H., et al., *Sensitivity of cell-based biosensors to environmental variables.* Biosensors and Bioelectronics, 2005. **20**(7): p. 1397-1406.
60. L. Giovangrandi, K.H.G., R. H. Whittington, and G. T.A. Kovacs, *Low-cost microelectrode array with integrated heater for extracellular recording of cardiomyocyte cultures using commercial flexible printed circuit technology.* Sensors and Actuators, 2006. **113**: p. 545-554.
61. Wu, J., Yuxing Ben, David Battigelli, and Hsueh-Chia Chang, *Long-Range AC Electroosmotic Trapping and Detection of Bioparticles.* Ind. Eng. Chem. Res., 2005. **44**: p. 2815-2822.
62. *Vimentin (Host: Mouse, Clone: V9) for IHC (Zymed®) Product description*, in *Online Catalog*, Sigma Invitrogen.
63. Naito, H., et al., *Optimizing Engineered Heart Tissue for Therapeutic Applications as Surrogate Heart Muscle.* Circulation, 2006. **114**(1_suppl): p. I-72-78.

6. APPENDIX

6.1. PROTOCOLS

6.1.1. Isolation of neonatal rat cardiomyocyte cells

1. Excise a whole heart from the rat and place it in cold HBSS buffer.
2. Remove the left and right atrium and blood vessels by using small scissors and forceps.
3. Quarter remaining heart ventricles and wash in HBSS buffer.
4. Digest quartered hearts in 25 ml of 0.06% (w/v) trypsin in HBSS buffer by shaking overnight at 4˚C.
5. Stop trypsin digestion by adding 10 ml of cardiac growth medium followed by incubation at 37 ˚C for 4 min with shaking at 150 rpm.
6. After discarding supernatant, add 10 ml of 0.1% (w/v) type II collagenase in HBSS to the tissue and incubate at 37˚C for 4 min with shaking at 150 rpm.
7. Collect the cell suspension from the digestion and wash the pellet with 10 ml of HBSS buffer and collect the supernatant.
8. Repeat steps 6 and 7 until no more tissue remains.
9. Centrifuge at 150 g for 10 min the pooled cell suspension from step 8 and then wash the cell pellet with 25 ml of cell culture medium to remove residual collagenase.
10. Resuspend the cells in the cell culture medium and pre-plate for 1 h to enrich cell suspension with cardiomyocytes by removing fibroblasts. In this step, fibroblasts will adhere to the culture dish within 1 h but most of cardiomyocytes will remain in suspension.
11. Harvest cells by centrifugation at 1200 rpm for 5 min.
12. Determine cell number and viability of cardiomyocytes by hemocytometer counts using trypan blue to exclude dead cells. Twenty neonatal rat hearts should yield 8-12 x 10^7 cells.

6.1.2. Preparation of C2C12 mouse myoblast cells

1. Remove a vial of frozen cell stock (cell concentration, 1x10e^6 cells/ml) from liquid N_2.
2. Make cell culture medium (growth medium and fusion medium) and leave it in water bath, 37°C, at least 10 minutes.

Growth medium: DMEM (in cold room, for c2c12 w/HEPES) +10% FBS +1% Pen/Strep.

Fusion medium: DMEM + 2% FBS + 1% Pen/Strep.

3. Quickly thaw the cells in water bath, add 5mL DMEM, mix with cells and centrifuge at 1200 RPM for 5 minutes. Remove excess fluids with Pasteur pipette. Then, resuspend with 1 ml of culture medium.
4. Transfer the cells into T-75 cell culture flask and add 10 ml fresh culture medium, and shake around a bit.
5. Incubate the flask at 5% CO2 in 37C humidified incubator.
6. The next day, change the media completely (to remove DMSO), by removing the media and add 10 ml of fresh media. Observe the cells.
7. At day 3 or 4, passage the cells.

6.1.3. Scaffold Preparation and Seeding

1. Cut the collagen scaffold into squares or rectangles of the desired size.
2. Immediately before use, hydrate each collagen scaffold in culture medium for 2 h in the 37°C at 5% CO_2 incubator.
3. Collect cells by centrifugation at 200 g for 10 min and resuspend in liquid Matrigel using 5 µl Matrigel per 1 million cells, while working on ice to prevent premature gelation.
4. Gently blot dry pre-wetted collagen scaffolds, and then pipette cell suspension in Matrigel evenly on the top surface of each scaffold. Inoculate each scaffold with freshly isolated heart cells at a density 1.35×10^8 cells/cm^3.
5. Gelation is complete within 15 min in a 37 °C incubator, and inoculated scaffolds are then transferred into a Petri dish.

6.1.4. Bioreactor Assembly

1. Prepare 10 g of the 10:1 mixture of PDMS and initiator. Pour 7 g of mixture into one 60-mm glass Petri dish and de-gas under vacuum for 1 h. Cure in oven at 65 °C for 2 h. The final thickness of PDMS is 0.3 cm, thick enough to hold pins in place, but thin enough to observe scaffolds with an inverted microscope.
2. Prepare an additional 60 g of the 10:1 mixture of PDMS and initiator, add 10 g to each well of a six-well plate, and cure. The final thickness of PDMS in each well will be 1.0 cm.

3. Remove PDMS disks (3.5 cm diameter) from well and cut in half. Use 3.0 mm biopsy punch to make 2 holes along linear surface, 1.0 mm from bottom edge, and corresponding to the desired electrode spacing.
4. Cut electrode rods to length of 5.0 cm.
5. Wrap wire multiple times around ends of each rod. For carbon rods, drill a small hole in end of rod and insert wire before wrapping. Leave an additional 10 cm of wire attached to each electrode.
6. Insert two rods into punched holes of one PDMS half-disk. On opposing end, insert rods into a second half-disk. Length of electrode exposed to electrolyte is 4.0 cm.
7. Place electrode/PDMS block into center of Petri dish with PDMS base. Electrode supports may need to be trimmed to fit.

6.1.5. EIS measurements of bioreactor

1. Take electrochemical impedance spectroscopy (EIS) measurements of electrodes in Petri dish with 20 ml of PBS. Acquire EIS spectra over a frequency range from 1 x 10^6 to 1 x 10^{-2} Hz with a perturbation amplitude of 10 mV.
2. Record for each frequency the real (resistive) and imaginary (capacitive) components of the impedance response, Z' and Z", respectively.
3. Evaluate data in ZView to generate Nyquist and Bode plots for each condition.
4. Create an "equivalent circuit" of the system using resistors and capacitors in series and in parallel (see Section 1.4.6 for a discussion of equivalent circuit parameters). Calculate the values for CPE, Rp and η using instant and manual fit functions in ZView software.

6.1.6. Current Measurement in the Bioreactor

1. Place 10 ohm resistance in series with the bioreactor in the stimulation loop. The value of this resistance is high enough to allow measurement of a voltage across the electrode, even with small current.
2. Apply the stimulus (e.g., 5 V, 2 ms square wave). Check with oscilloscope that intended waveform is faithfully applied to bioreactor. If not, current limit of stimulator may be exceeded and corrective action must be taken (e.g., electrode area or medium conductivity reduced or current rating of stimulator increased).

3. Record over time the voltage across the resistor with the oscilloscope, and for each time point, calculate the value of current by dividing the voltage across the resistor by the resistance value (Ohm's law).
4. Calculate the total amount of injected charge by integrating the current profile for the duration of the stimulus. Current profiles and calculated injected charge for electrodes of different materials (carbon, stainless steel, titanium, and titanium nitride) are shown in **Figure 14**.

6.1.7. Choice of the Electrode Material

1. Calculate the power spectral density of the stimulus waveform to determine the frequency band that concentrates most of the energy in the pulse. For 5 V, 2 ms square pulses delivered at 1 Hz it is the frequency band below 1 kHz (see **Figure 15**).
2. Analyze the Bode plot to determine the behavior of the electrode material within this frequency band. For example, the carbon electrodes we use have a corner frequency of approximately 10 Hz, and so the electrode behaves as both a capacitor below this frequency and a resistor above this frequency. Therefore, we must consider both the electrode's CPE and R_p values (see **Figure 10**).
3. Compare CPE, R_p and injected charge values calculated from EIS for different electrodes. Choose electrode material with high CPE to increase the amount of charge injection (as CPE increases, the amount of charge storage on the electrode increases), and high R_p to reduce corrosive currents and therefore harmful reactions.

6.1.8. Electrical Simulation of Construct

1. Place three scaffolds between electrodes in prepared 60 mm Petri dish (see **Section 2.2** for bioreactor assembly). Fix scaffold position with two stainless steel pins bent over scaffold and into PDMS base layer (see **Figure 6**). These pins should not touch each other nor the electrodes in order to minimally interfere with the electric field.
2. Add 15 ml of cardiac medium to Petri dish and place in incubator (37 °C, 5% CO_2).
3. Make electrical connections with an effort to prevent any undesired electrical connections via metal or electrolyte. Place a layer of autoclave paper beneath all bioreactors to prevent unintentional electrical

connections via moisture in the bioreactor or via metal parts within the incubator.

4. Stimulate with monophasic 2 ms duration square pulses delivered at 1 Hz. Start electrical stimulation 3 days after seeding scaffolds with isolated heart cells.
5. Stop electrical stimulation 8 days after seeding scaffolds (5 days of electrical stimulation).

6.1.9. Contractile Activity

1. Place each construct between two carbon electrodes connected to a cardiac stimulator in a 60-mm Petri dish filled with 15 ml cardiac growth medium.
2. Maintain the temperature of the Petri dish at 37 °C.
3. Place the entire setup on an optical microscope, and monitor contractile responses to electrical stimuli (rectangular pulses, 2 ms duration) using 2x magnification.
4. Increase signal amplitude in 0.1 V increments up to 10 V,
5. Measure two parameters to evaluate the contractile behavior in response to electrical stimulation: excitation threshold, ET (the minimum voltage of electrical stimulation required to elicit sustained synchronous contractions of tissue constructs at a frequency of 60 bpm) and maximum capture rate, MCR (maximum frequency of sustained synchronous contractions that can be achieved at a stimulation voltage corresponding to 1.5 ET).

6.1.10. Histological Analysis

1. Deparafinize sections to retrieve antigen by heat treatment for 20 min at 95°C in a decloacking chamber (Biocare Medical, Concord, CA).
2. Subsequently, block sections with 10% horse serum for 30 min at room temperature in a humidified chamber.
3. Incubate the sections for 1 h at 37 °C with either rabbit anti-cardiac troponin I or rabbit anti-connexin 43 (Cx43) diluted in PBS containing 0.5% Tween 20 and 1.5% horse serum.
4. Incubate sections at RT, first for 30 min with the secondary antibody (mouse anti-rabbit).
5. Assess construct architecture and cell distribution from the stained sections using fluorescent microscope (Axioplan, Zeiss, Thornwood, NY).

6.1.11. Ultrastructure Analysis

1. Wash scaffolds in PBS by placing each scaffold in a single well of a 96-well plate and soaking 3 times for 5 minutes each in 200 μL of solution.
2. transfer each scaffold to clean wells of the 96-well plate and subsequently, block sections with 200 μL of 10% horse serum for 40 min at room temperature.
3. Apply the primary antibody of choice at the proper concentration and incubate scaffolds in 200 μL of solution diluted in PBS containing 0.5% Tween 20 and 1.5% horse serum in a humidified chamber at 37C for 1 hr.
4. Wash scaffolds in PBS 3 times for 5 min. each.
5. Apply the secondary antibody of choice at the proper concentration and incubate scaffolds in 200 μL of solution in a humidified chamber at 37C for 30 min.
6. Apply nuclear stain of choice (Topro-III for confocal microscope utilized in this study).